J. Fluid Mech. (1994), *vol.* 264, *pp.* 213–254

Direct numerical simulation of passive control of three-dimensional phenomena in boundary-layer transition using wall heating

By L. D. KRAL† AND H. F. FASEL

Department of Aerospace and Mechanical Engineering, University of Arizona, Tucson, AZ 85721, USA

(Received 12 July 1991 and in revised form 7 September 1993)

A numerical model is presented for investigating control of the three-dimensional boundary-layer transition process. Control of a periodically forced, spatially evolving boundary layer in water is studied using surface heating techniques. The Navier–Stokes and energy equations are integrated using a fully implicit finite difference/spectral method. The Navier–Stokes equations are used in vorticity–velocity form and are coupled with the energy equation through the viscosity dependence on temperature. Passive control of small amplitude two-dimensional waves and three-dimensional oblique waves is numerically simulated with either uniform or non-uniform wall heating applied. Both amplitude levels and amplification rates are strongly reduced with heating applied. Comparison is made with parallel and non-parallel linear stability theory and experiments. Control of the early stages of the nonlinear breakdown process is also investigated using uniform wall heating. Both control of the fundamental and subharmonic routes to turbulence are investigated. For both breakdown processes, a strong reduction in amplitude levels and growth rates results. In particular, the high three-dimensional growth rates that are characteristic of the secondary instability process are significantly reduced below the uncontrolled levels.

1. Introduction

Delay of the boundary-layer transition process can significantly reduce the skin friction or viscous drag. A sizeable decrease in the viscous drag forces has the potential to appreciably reduce fuel consumption and allow greater range and speed. According to Bushnell (1983) and Bushnell & Hefner (1990), drag caused by the formation of the viscous boundary layer accounts for approximately 30–40 % of the drag of high-speed aircraft and missiles, 50 % of the drag on transport aircraft and surface ships, and 70 % of the drag of underwater bodies.

In low-disturbance boundary-layer flows, the first stage of the transition to turbulent motion begins with the development of small-amplitude Tollmien–Schlichting waves. As the amplitudes of the instability waves exceed certain threshold values, nonlinear effects become appreciable and three-dimensional structures appear. The occurrence of three-dimensional phenomena has been observed experimentally in detail by Klebanoff, Tidstrom & Sargent (1962), Hama & Nutant (1963), and Kovasznay, Komoda & Vasudeva (1962). The three-dimensional structure that evolves is characterized by spanwise alternating peaks and valleys, or regions of enhanced and reduced wave

† Present address: McDonnell Douglas Aerospace, PO Box 516, MC 106-4126, St Louis, MO 63166, USA.

amplitude, and an associated system of streamwise vortices. This route to transition is called fundamental breakdown because the three-dimensional wave components have the same frequency as the fundamental two-dimensional wave component. In contrast, a second route to transition in the boundary layer has been observed by Kachanov & Levchenko (1984), Saric, Kozlov & Levchenko (1984), and Saric & Thomas (1983). This route is characterized by subharmonic three-dimensional disturbances which leads to a peak and valley system that is staggered. The streamwise wavelength of the three-dimensional structures is twice the wavelength of the fundamental wave. The experiments indicate that subharmonic breakdown occurs for low and intermediate amplitudes of the two-dimensional wave, while the fundamental breakdown occurs for higher amplitudes.

For small freestream disturbance levels, the Tollmien–Schlichting regime covers by far the largest downstream distance of the entire transition region. For technical applications of transition control, this region is particularly amenable to manipulations of the transition process. The flow is easier to control in the early nonlinear stages of transition than the later strongly nonlinear stages. Full transition appears to be inevitable once the strongly nonlinear stage has been reached. Thus efforts to prevent or delay transition applied at the early stages should prove more successful.

There are basically two approaches to control the transition process. The first approach is based on the idea of modifying the base flow and thus its stability characteristics. The critical Reynolds number at which the flow becomes unstable is either increased or reduced. This approach is often characterized as passive control. Several techniques have proved to be effective for passive control including pressure gradients, wall suction/blowing, and heating/cooling. The second approach to influence the transition process is active (or reactive) control in which the disturbance flow resulting from the instability of the base flow is directly influenced using wave superposition techniques. An investigation of active control simulating surface heater strips as in the experiments of Liepmann, Brown & Nosenchuck (1982) has been made by Kral & Fasel (1991) using the complete Navier–Stokes equations. In the present paper, passive control using surface heating techniques is investigated. In particular, we are investigating in detail the effect of wall heating for both primary (Tollmien–Schlichting) instability and secondary (three-dimensional) disturbances. Experiments have been conducted only for control of small-amplitude, two-dimensional instability waves, whereas in the present numerical investigations control of large-amplitude two-dimensional and three-dimensional waves using surface heating is studied.

The effects of passive wall heating were investigated as early as 1946 by Liepmann & Fila (1946) who have shown experimentally that wall heating in air hastens transition. Hauptmann (1968) used a perturbation procedure to predict that wall heating leads to appreciable stabilization in water and slight destabilization in air for small variations in viscosity. The first numerical results of heated and cooled water boundary layers were obtained by Wazzan, Okamura & Smith (1968, 1970*a*, *b*). They formulated a linear stability theory model which included the effects of viscosity variation with temperature in the base flow and obtained neutral stability curves for several levels of heating and cooling. Lowell (1974) reformulated the linear stability problem for a wall-heated boundary layer by including all fluid property variations in the boundary layer along with the disturbance energy equation, thus allowing fluid property fluctuations as well as temperature fluctuations. Lowell found his results to be somewhat insensitive to the thermal disturbances and the viscosity variation with temperature for the mean flow has by far the most significant impact on the stability

of the flow. Stabilization of water boundary layers has been demonstrated experimentally by Strazisar, Reshotko & Prahl (1977), Barker & Jennings (1977), Barker (1979), and Nosenchuck (1982). Barker & Jennings and Barker studied the boundary-layer flow on the inside of a cylindrical tube and found a considerable increase in transition Reynolds number with heating. Nosenchuck found the same overall trends as Barker & Jennings and Barker, although Nosenchuck's experimental results showed less stabilization. This discrepancy was attributed to a slight favourable pressure gradient in the tube flow of Barker. The results of Strazisar, Reshotko & Prahl show that as wall heating is increased the minimum critical Reynolds number at which the flow becomes unstable increases, the disturbance growth rates decrease, and the region of unstable frequencies decreases. These trends are consistent with the numerical analysis of Wazzan, Okamura & Smith and Lowell. Differences between the experimental data and numerical results were attributed to non-parallel effects. El-Hady & Nayfeh (1979) have performed a non-parallel stability analysis using the method of multiple scales. Bestek, Dittrich & Fasel (1987) have numerically studied passive control by surface heating for a two-dimensional, incompressible, spatially evolving boundary layer using the complete Navier–Stokes equations. Although, direct comparison with experiments was not made, the numerical trends were consistent with experimental results.

In addition to uniformly heating the flat plate, Strazisar & Reshotko (1978), Barker & Jennings (1977), and Nosenchuck (1982) have experimentally examined non-uniform surface temperature distributions. More efficient heat utilization can be achieved using non-uniform wall heating since the flow upstream of the critical Reynolds number is stable and does not need heating. Gazley & Wazzan (1985) have also studied a non-uniform surface temperature distribution using the linear stability theory model of Wazzan, Okamura & Smith. Nayfeh & El-Hady (1980) and Asrar & Nayfeh (1985) performed stability analyses showing that the stability is strongly dependent on the non-uniform heat distribution.

Zang & Hussaini (1985*a*, *b*) have examined three-dimensional passive control of the secondary instability process using heating, suction, and pressure gradient by direct numerical simulation of the boundary layer using the temporal model. They investigated control of the fundamental breakdown process and found that passive control did not prevent secondary instability. However, the secondary instability process is substantially weaker than for the uncontrolled boundary layer. In contrast, in this paper, transition control is investigated numerically based on a spatial model. This model allows for investigations of spatially growing, three-dimensional disturbance waves in a growing two-dimensional boundary layer. With this model, the three-dimensional hydrodynamic stability of an initially laminar, incompressible boundary layer on a flat plate with constant surface heating applied can be investigated. The unsteady, three-dimensional Navier–Stokes and energy equations are the basic equations used in this model.

A numerical model based on the complete Navier–Stokes equations that allowed for two-dimensional numerical simulations of spatially growing and propagating small-amplitude Tollmien–Schlichting waves in a boundary layer was first introduced by Fasel (1976). Based on the same numerical model, Fasel, Bestek & Schefenacker (1977) have performed calculations with larger-amplitude oscillations to investigate nonlinear effects in the two-dimensional stages of boundary-layer transition. A modified version of this numerical method was used by Fasel & Bestek (1980) to study the nonlinear two-dimensional transition behaviour in plane Poiseuille flow. Later, Fasel, Rist & Konzelmann (1990) developed a numerical method, also based on the complete

Navier–Stokes equations, to investigate spatial three-dimensional disturbances evolving in a two-dimensional boundary layer. This numerical model was adapted for the investigation of three-dimensional boundary-layer transition control which is the subject of this paper. The numerical model had to be extended to include the energy equation and to allow for temperature-dependent viscosity.

In order to gain an understanding of the control aspects of transition, linear small-amplitude disturbances were first considered in the present study. Therefore, control of small-amplitude two-dimensional waves and three-dimensional oblique waves was studied first. Uniform and non-uniform surface temperature distributions were considered. The results are compared with available experimental measurements and theory. Control of the nonlinear secondary instability process was also investigated with uniform heating applied. Results of control of both the fundamental peak–valley and the subharmonic staggered peak–valley breakdown processes are discussed.

2. Governing equations

The flow of a non-isothermal viscous fluid is governed by the Navier–Stokes and energy equations. Water is chosen as the representative fluid throughout this work so that comparison with the results of previous experimental and theoretical investigations can be made. An assessment of the influence of the various force, energy, and variable property effects on the flow considered in this paper was made by Kral (1988). Here, buoyancy forces and viscous dissipation (frictional heat) are neglected for the moderate velocities considered. For water, the fluid properties are not affected by moderate pressures. The specific heat and density are relatively independent of temperature and the thermal conductivity also varies little with temperature in water. However, the viscosity of water decreases very markedly with increasing temperature and therefore the variation of viscosity with temperature is included.

2.1. *Equations of motion in vorticity–velocity representation*

The numerical method is based on the Navier–Stokes equations in a vorticity–velocity formulation. This formulation was first used successfully for transition simulations by Fasel (1976). The equations are made dimensionless by choosing characteristic scales that correspond with the physical scales of the problem considered. The variables are non-dimensionalized as follows:

$$x = \frac{\bar{x}}{\bar{L}}, \qquad y = \frac{\bar{y}}{\bar{L}} Re^{\frac{1}{2}}, \qquad z = \frac{\bar{z}}{\bar{L}},$$

$$u = \frac{\bar{u}}{\bar{U}_\infty}, \qquad v = \frac{\bar{v}}{\bar{U}_\infty} Re^{\frac{1}{2}}, \qquad w = \frac{\bar{w}}{\bar{U}_\infty},$$

$$t = \frac{\bar{t}\bar{U}_\infty}{\bar{L}}, \qquad T = \frac{\bar{T}-\bar{T}_\infty}{\bar{T}_w-\bar{T}_\infty}, \qquad \mu = \frac{\bar{\mu}}{\bar{\mu}_\infty},$$

$$\omega_x = \frac{\bar{\omega}_{\bar{x}}\bar{L}}{\bar{U}_\infty Re^{\frac{1}{2}}}, \quad \omega_y = \frac{\bar{\omega}_{\bar{y}}\bar{L}}{\bar{U}_\infty}, \qquad \omega_z = \frac{\bar{\omega}_{\bar{z}}\bar{L}}{\bar{U}_\infty Re^{\frac{1}{2}}},$$

where the subscript 'w' represents the wall value, the subscript '∞' represents the free-stream value and $\bar{L}$ is a characteristic length. The parameter $Re = \bar{\rho}\bar{U}_\infty \bar{L}/\bar{\mu}_\infty$ is the Reynolds number. The y-coordinate and normal velocity component v are stretched by the factor $Re^{\frac{1}{2}}$ to ensure that all coordinates and velocity components are of the same order of magnitude in the numerical computations.

For the incompressible, three-dimensional flow of a Newtonian fluid, the non-dimensional conservation laws are (in vector notation).

Continuity:
$$\nabla_1 \cdot U = 0, \tag{2.1}$$

Vorticity transport:
$$\frac{D\omega}{Dt} - (\omega \cdot \nabla_1) U = \mu \nabla_1^2 \omega + c. \tag{2.2}$$

Energy:
$$\frac{DT}{Dt} = \frac{1}{Re\,Pr} \nabla_1^2 T, \tag{2.3}$$

where the components of the vector $c = [c_x, c_y, c_z]$ are given by

$$c_x = +\frac{1}{Re}\frac{\partial \mu}{\partial x}\left(\frac{\partial \omega_x}{\partial x}\right) - \frac{\partial \mu}{\partial y}\left(\frac{1}{Re}\frac{\partial \omega_y}{\partial x} - 2\frac{\partial \omega_x}{\partial y}\right) + \frac{1}{Re}\frac{\partial \mu}{\partial z}\left(2\frac{\partial \omega_x}{\partial z} - \frac{\partial \omega_z}{\partial x}\right) - \frac{1}{Re}\frac{\partial^2 \mu}{\partial x\,\partial y}\left(\frac{\partial u}{\partial z} + \frac{\partial w}{\partial x}\right)$$
$$- \frac{2}{Re}\frac{\partial^2 \mu}{\partial y\,\partial z}\left(\frac{\partial \omega}{\partial z} - \frac{\partial v}{\partial y}\right) + \frac{1}{Re}\frac{\partial^2 \mu}{\partial x\,\partial z}\left(\frac{\partial u}{\partial y} + \frac{1}{Re}\frac{\partial v}{\partial x}\right) - \left(\frac{\partial^2 \mu}{\partial y^2} - \frac{1}{Re}\frac{\partial^2 \mu}{\partial z^2}\right)\left(\frac{1}{Re}\frac{\partial v}{\partial z} + \frac{\partial w}{\partial y}\right), \tag{2.4a}$$

$$c_y = +\frac{\partial \mu}{\partial x}\left(\frac{2}{Re}\frac{\partial \omega_y}{\partial x} - \frac{\partial \omega_x}{\partial y}\right) + \frac{\partial \mu}{\partial y}\left(\frac{\partial \omega_y}{\partial y}\right) - \frac{\partial \mu}{\partial z}\left(\frac{\partial \omega_z}{\partial y} - \frac{2}{Re}\frac{\partial \omega_y}{\partial z}\right) + \frac{\partial^2 \mu}{\partial x\,\partial y}\left(\frac{1}{Re}\frac{\partial v}{\partial z} + \frac{\partial w}{\partial y}\right)$$
$$- \frac{\partial^2 \mu}{\partial y\,\partial z}\left(\frac{\partial u}{\partial y} + \frac{1}{Re}\frac{\partial v}{\partial x}\right) - \frac{2}{Re}\frac{\partial^2 \mu}{\partial x\,\partial z}\left(\frac{\partial u}{\partial x} - \frac{\partial w}{\partial z}\right) - \left(\frac{1}{Re}\frac{\partial^2 \mu}{\partial z^2} - \frac{\partial^2 \mu}{\partial x^2}\right)\left(\frac{\partial u}{\partial z} + \frac{\partial w}{\partial x}\right), \tag{2.4b}$$

$$c_z = -\frac{1}{Re}\frac{\partial \mu}{\partial x}\left(\frac{\partial \omega_x}{\partial z} - \frac{\partial \omega_z}{\partial x}\right) + \frac{\partial \mu}{\partial y}\left(2\frac{\partial \omega_z}{\partial y} - \frac{1}{Re}\frac{\partial \omega_y}{\partial z}\right) + \frac{1}{Re}\frac{\partial \mu}{\partial z}\left(\frac{\partial \omega_z}{\partial z}\right) - \frac{2}{Re}\frac{\partial^2 \mu}{\partial x\,\partial y}\left(\frac{\partial v}{\partial y} - \frac{\partial u}{\partial x}\right)$$
$$+ \frac{1}{Re}\frac{\partial^2 \mu}{\partial y\,\partial z}\left(\frac{\partial u}{\partial z} - \frac{\partial w}{\partial x}\right) - \frac{1}{Re}\frac{\partial^2 \mu}{\partial x\,\partial z}\left(\frac{1}{Re}\frac{\partial v}{\partial z} + \frac{\partial w}{\partial y}\right) - \left(\frac{1}{Re}\frac{\partial^2 \mu}{\partial x^2} - \frac{\partial^2 \mu}{\partial y^2}\right)\left(\frac{\partial u}{\partial y} + \frac{1}{Re}\frac{\partial v}{\partial x}\right). \tag{2.4c}$$

The Prandtl number is defined as $Pr = \bar{\mu}_\infty \bar{c}_\infty / \bar{k}_\infty$.

The velocity and vorticity components are related through three Poisson-type equations that are derived by relating the three velocity components to the three components of vorticity. The three Poisson equations are

$$\nabla_2^2 u = -\frac{\partial \omega_y}{\partial z} - \frac{\partial^2 v}{\partial x\,\partial y}, \tag{2.5}$$

$$\nabla_1^2 v = \frac{\partial \omega_x}{\partial z} - \frac{\partial \omega_z}{\partial x}, \tag{2.6}$$

$$\nabla_2^2 w = \frac{\partial \omega_y}{\partial x} - \frac{\partial^2 v}{\partial y\,\partial z}. \tag{2.7}$$

The velocity U and vorticity ω are vector fields: $U = [u, v, w]$ and $\omega = [\omega_x, \omega_y, \omega_z]$ where ω is defined by $\omega = -\nabla \times U$. The non-dimensional vorticity components are then defined by

$$\omega_x = \frac{1}{Re}\frac{\partial v}{\partial z} - \frac{\partial w}{\partial y}, \tag{2.8a}$$

$$\omega_y = \frac{\partial w}{\partial x} - \frac{\partial u}{\partial z}, \tag{2.8b}$$

$$\omega_z = \frac{\partial u}{\partial y} - \frac{1}{Re}\frac{\partial v}{\partial x}. \tag{2.8c}$$

The non-dimensional form of the vector operators are

$$\nabla_1 = \frac{\partial}{\partial x}\boldsymbol{i} + \frac{\partial}{\partial y}\boldsymbol{j} + \frac{\partial}{\partial z}\boldsymbol{k}, \tag{2.9a}$$

$$\nabla_2 = \frac{\partial}{\partial x}\boldsymbol{i} + Re^{\frac{1}{2}}\frac{\partial}{\partial y}\boldsymbol{j} + \frac{\partial}{\partial z}\boldsymbol{k}, \tag{2.9b}$$

$$\nabla_1^2 = \frac{\partial^2}{\partial x^2} + Re\frac{\partial^2}{\partial y^2} + \frac{\partial^2}{\partial z^2}, \tag{2.9c}$$

$$\nabla_2^2 = \frac{\partial^2}{\partial x^2} + \frac{\partial^2}{\partial z^2}. \tag{2.9d}$$

A detailed derivation of these equations is given in Kral (1988).

For the numerical method, (2.2)–(2.7) are used. The continuity equation (2.1) is not directly solved in the field. However, the divergence of the velocity field is used to monitor the quality of the numerical solution and provides a check on the grid resolution required. This check on the divergence was shown by Kral (1988) and revealed that the divergence-free condition was well satisfied. Thus, the governing equations are a system of seven equations for the eight components u, v, w, ω_x, ω_y, ω_z, T, and μ. To relate viscosity and temperature, $\mu = \mu(T)$, the empirical relationships of Hardy & Cottington (1949) and Swindells (1982) are employed. The empirical relationship is for 0 °C $\leqslant \bar{T} \leqslant$ 20 °C:

$$\log_{10}\bar{\mu}_{\bar{T}} = \frac{1301}{998.333 + 8.1855(\bar{T}-20) + 0.00585(\bar{T}-20)^2} - 1.30233, \tag{2.10a}$$

for 20 °C $\leqslant \bar{T} \leqslant$ 100 °C:

$$\log_{10}\frac{\bar{\mu}_{\bar{T}}}{\bar{\mu}_{20}} = \frac{1.3272(20-\bar{T}) - 0.001053(\bar{T}-20)^2}{\bar{T}+105}, \tag{2.10b}$$

where temperature is in degrees Celsius, viscosity is in centipoise, and $\bar{\mu}_{20} = 1.002$ CP.

3. Boundary and initial conditions

To complete the mathematical formulation of the problem, an integration domain has to be identified and the boundary conditions on the boundaries have to be specified. Matters are more complicated here because the spatial development of the flow is of interest. In 'flow-through' systems, physically realistic inflow and outflow boundary conditions are difficult to prescribe and implement in the numerical method. For a discussion conceiving difficulties resulting from the simulations based on the realistic (spatial) inflow–outflow model see Fasel (1989). The numerical simulations are organized such that, first the steady, laminar, two-dimensional solution of the governing equations is obtained for the heated, undisturbed flow whose stability is to be investigated. A time-dependent method is used to solve for the undisturbed, mean flow by integrating the unsteady Navier–Stokes equations until a steady-state solution is obtained. Then, periodic perturbations are introduced and the time-dependent, three-dimensional solutions to the governing equations are calculated. The spatial domain for the investigations considered in this work is rectangular as shown schematically in figure 1.

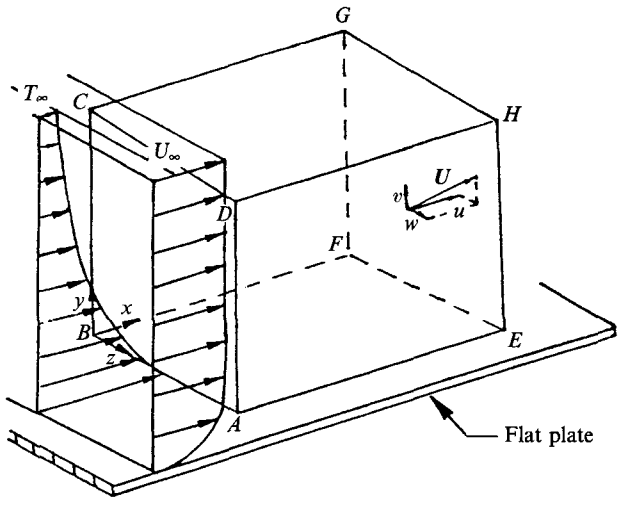

FIGURE 1. Computational domain and coordinate system.

3.1. *Boundary and initial conditions for the undisturbed flow*

For a boundary-layer flow along a flat plate, the typical velocity profile used in stability analyses is the similarity solution of the boundary-layer equations. For the case of isothermal flow, the well-known Blasius boundary-layer profile can be used. For a uniform wall temperature distribution or for a power law temperature distribution ($T_w(x) - T_\infty = Ax^p$) in a fluid with constant properties, the flow profiles are still self-similar. However, for a fluid with variable properties, the flow is no longer self-similar if the wall temperature is non-uniform.† The similarity solutions of the momentum and energy equations with variable viscosity and a uniform wall temperature distribution are used to specify the inflow boundary conditions for the two-dimensional undisturbed flow. The velocity, vorticity, and temperature components for this similarity solution are denoted by the subscript '*SIM*', thus, $u_{SIM}(x,y)$, $v_{SIM}(x,y)$, $\omega_{zSIM}(x,y)$, and $T_{SIM}(x,y)$.

The complete set of boundary and initial conditions for the undisturbed flow are given below. Since the undisturbed flow is two-dimensional, the z-velocity component w and the ω_x and ω_y vorticity components vanish. Also, boundary conditions on the lateral faces of the domain (*B-F-G-C*) and (*A-E-H-D*) are not needed.

Initial conditions for the undisturbed flow

The steady-state solution to the governing equations can be obtained for any initial velocity, vorticity, and temperature distribution. However, computational time is significantly reduced if the initial conditions are close to the steady-state solution. Therefore, the similarity solution is used to initialize the field for the undisturbed flow:

$$\hat{\phi}(x,y,z,0) = \phi_{SIM}(x,y), \tag{3.1}$$

where $\hat{\phi} = [\hat{u}, \hat{v}, 0, 0, 0, \hat{\omega}_z, \hat{T}]$ and the superscript '^' represents the undisturbed flow.

† Nayfeh & El-Hady (1980) state that non-similar boundary-layer profiles are necessary in a stability analysis of non-uniform wall temperature distributions to agree even qualitatively with experimental data. In this work, the undisturbed flow is a solution of the full Navier–Stokes and energy equations and is thus a non-similar solution.

Inflow boundary conditions for the undisturbed flow

The similarity solution for the flat plate boundary layer is imposed at the inflow plane (*A-B-C-D*) as already discussed:

$$\hat{\phi}(x_0, y, z, t) = \phi_{SIM}(x_0, y). \tag{3.2}$$

Outflow boundary conditions for the undisturbed flow

At the outflow plane (*E-F-G-H*), boundary conditions are imposed so as to minimize the upstream influence on the flow. Conditions that were satisfactory with this regard are:

$$\frac{\partial \hat{u}}{\partial x}(x_N, y, z, t) = -\frac{\partial v}{\partial y}(x_N, y, z, t), \tag{3.3a}$$

$$\frac{\partial^2 \hat{v}}{\partial x^2}(x_N, y, z, t) = 0, \tag{3.3b}$$

$$\frac{\partial^2 \hat{\omega}_z}{\partial x^2}(x_N, y, z, t) = 0, \tag{3.3c}$$

$$\frac{\partial^2 \hat{T}}{\partial x^2}(x_N, y, z, t) = 0. \tag{3.3d}$$

These conditions result from boundary-layer considerations and from the continuity equation. For large Reynolds numbers, the $\partial^2/\partial x^2$ terms in the governing equations are negligible. If the terms were neglected everywhere, the equations would become parabolic with respect to x. For the present investigation with the full Navier–Stokes equations, the terms are neglected only at the outflow boundary for the v Poisson, vorticity, and energy equations. Boundary condition (3.3*a*) is used to enforce mass conservation at the outflow boundary.

Outer boundary conditions for the undisturbed flow

The boundary conditions at the outer boundary (*D-C-G-H*) are:

$$\hat{u}(x, y_M, z, t) = 1, \tag{3.4a}$$

$$\frac{\partial \hat{v}}{\partial y}(x, y_M, z, t) = 0, \tag{3.4b}$$

$$\hat{\omega}_z(x, y_M, z, t) = 0, \tag{3.4c}$$

$$\hat{T}(x, y_M, z, t) = 0. \tag{3.4d}$$

Equation (3.4*a*) denotes that there is no free-stream pressure gradient imposed on the flow. Equation (3.4*b*) is derived from the continuity equation and taking (3.4*a*) into account. Condition (3.4*c*) is based on the physical consideration that the vorticity is confined to the region of high shear close to the wall. Condition (3.4*d*) is also based on physical considerations. The thermal boundary layer for water ($Pr = 6.3$) is much smaller than the fluid boundary layer and therefore the temperature gradients are confined to the wall region as well.

Wall boundary conditions for the undisturbed flow

At the wall (*A-B-F-E*), the conditions for the undisturbed flow are:

$$\hat{u}(x,0,z,t) = 0, \tag{3.5a}$$

$$\hat{v}(x,0,z,t) = 0, \tag{3.5b}$$

$$\frac{\partial \hat{v}}{\partial y}(x,0,z,t) = 0, \tag{3.5c}$$

$$\frac{\partial \hat{\omega}_z}{\partial x}(x,0,z,t) = -\frac{\partial^2 \hat{v}}{\partial y^2}, \tag{3.5d}$$

$$\hat{T}(x,0,z,t) = A_0 x^p. \tag{3.5e}$$

Boundary condition (3.5*a*) is the no-slip condition and (3.5*b*) models an impermeable wall. Boundary condition (3.5*c*) results from the continuity equation and is used as an integral condition for boundary condition (3.5*d*). The boundary condition for the wall vorticity, (3.5*d*), is derived by applying the v Poisson equation at the wall. Previous stability investigations by Fasel (1976) have shown that use of this boundary condition for the vorticity yields numerical results which are in excellent agreement with linear stability theory and experimental investigations.

Finally, for the wall temperature, boundary condition (3.5*e*) is imposed. This condition depends on the mode of control under investigation. The coefficient A_0 denotes the level of heating and the wall temperature can be varied with the function x^p. For $A_0 = 0$, the wall is unheated. For $A_0 \neq 0$ and $p = 0$, a uniform wall temperature distribution is imposed. For $A_0 \neq 0$ and $p \neq 0$, a non-uniform wall temperature distribution is used.

3.2 *Boundary and initial conditions for the disturbed flow*

The calculation of the disturbed flow is fundamentally different from that of the undisturbed flow and requires different boundary conditions to the steady flow. The conditions described below allow for generating three-dimensional periodic disturbances.

Initial conditions for the disturbed flow

The two-dimensional steady state solution provides the initial condition at time $t = t_1$ for the time integration of the disturbed flow, thus

$$\phi(x,y,z,t_1) = \hat{\phi}(x,y), \tag{3.6}$$

where $\phi = [u, v, w, \omega_x, \omega_y, \omega_z, T]$. The disturbances are then generated at $t > t_1$ using periodic wall heating or periodic suction and blowing. This boundary condition is imposed at the wall and is discussed together with the wall boundary conditions for the disturbed flow.

Lateral boundary conditions for the disturbed flow

The flow is assumed to be spanwise periodic. Thus, the periodicity conditions on the lateral boundaries (*A-D-H-E*) and (*B-C-G-F*) are:

$$\phi(x,y,0,t) = \phi(x,y,z_k,t). \tag{3.7}$$

Inflow boundary conditions for the disturbed flow

At the inflow plane (*A-B-C-D*), all disturbances are assumed to be zero.

$$\phi(x_0, y, z, t) = 0. \tag{3.8}$$

Outflow boundary conditions for the disturbed flow

The specification and implementation of proper outflow boundary conditions represent the major difficulty when developing a numerical method based on the spatial model. Ideally, radiation conditions are desired which render the outflow boundary transparent to all disturbance wave components. Often, wave reflection is a large problem in numerical simulations when finite computational domains are used. Recently Kloker, Konzelmann & Fasel (1993) have developed an effective method to prevent reflections by suppressing the disturbances in a 'relaminarization zone'.

To avoid problems resulting from wave reflections, an integration domain is used where the outflow boundary is propagated ahead of the disturbance wavefront in this work. The moving boundary is propagated sufficiently ahead of the disturbance waves such that no disturbances reach the outflow boundary. The choice of a moving boundary, instead of a large integration domain for the entire time integration, makes the simulations computationally more efficient. The boundary is propagated downstream using the following relationship:

$$x_0 < x_B = x_{B_1} + V_B(t - t_1) \leqslant x_N \quad \text{for } t \geqslant t_1, \tag{3.9}$$

where x_B is the position of the right-hand boundary, x_{B_1} is the position at time t_1, and V_B is the propagation speed of the right-hand boundary. If the outflow boundary position reaches its maximum, $x_B = x_N$, the boundary remains fixed thereafter. (Note: For the computation of the undisturbed flow, the outflow boundary is fixed at $x_B = x_N$.) However, results from the computation are only used for further analysis when the disturbance wavefront has not yet reached the outflow boundary in order to avoid contamination of the data owing to possible reflections. In typical calculations, the outflow boundary is six to seven wavelengths ahead of the wavefront and is propagated at a speed slightly greater than that of the disturbance waves.

Outer boundary conditions for the disturbed flow

At the free-stream boundary (*C-D-H-G*), exponential decay for the v velocity component is assumed:

$$\frac{\partial v}{\partial y}(x, y_M, z, t) = -\frac{\alpha^*}{Re^{\frac{1}{2}}} v(x, y_M, z, t), \tag{3.10a}$$

where α^* is a wavenumber. The choice of α^* is discussed later in context with the numerical method. The boundary conditions for the vorticity and temperature are

$$\omega(x, y_M, z, t) = 0, \tag{3.10b}$$

$$T(x, y_M, z, t) = 0. \tag{3.10c}$$

Boundary conditions (3.10*b*) and (3.10*c*) follow from the same considerations as for the undisturbed flow. Vorticity and temperature gradients are concentrated in the region near the wall and the free-stream boundary is far enough from the wall so that these quantities can be assumed to be zero. Note that only a boundary condition for the v velocity component is prescribed for the velocity field, as the u Poisson and w Poisson equations contain no y-derivatives for the u-velocity and w-velocity.

Wall boundary conditions for the disturbed flow

The disturbances are introduced into the integration domain at the wall (*A-B-F-E*) by superimposing on the steady flow a periodic perturbation. These perturbations are introduced into the domain using one of two different techniques. In the first technique, localized time-dependent normal velocity fluctuations are introduced within a narrow strip. In the second technique, localized time-dependent heating on a finite-width heating strip creates the perturbations. The following boundary conditions at the wall are then imposed:

$$u(x,0,z,t) = 0, \tag{3.11a}$$

$$v(x,0,z,t) = v_w(x,z,t), \tag{3.11b}$$

$$w(x,0,z,t) = 0, \tag{3.11c}$$

$$\frac{\partial^2\omega_x}{\partial x^2}(x,0,z,t)+\frac{\partial^2\omega_x}{\partial z^2}(x,0,z,t) = -\frac{\partial^2\omega_y}{\partial x\,\partial y}(x,0,z,t)+\frac{1}{Re}\frac{\partial}{\partial z}(\nabla_1^2 v(x,0,z,t)), \tag{3.11d}$$

$$\omega_y(x,0,z,t) = 0, \tag{3.11e}$$

$$\frac{\partial\omega_z}{\partial x}(x,0,z,t) = \frac{\partial\omega_x}{\partial z}(x,0,z,t)-\frac{1}{Re}\nabla_1^2 v(x,0,z,t), \tag{3.11f}$$

$$T(x,0,z,t) = T_w(x,z,t). \tag{3.11g}$$

Equations (3.11*a*) and (3.11*c*) are the no-slip conditions. The v velocity component at the wall is described by equation (3.11*b*). This condition allows for the introduction of localized streamwise, spanwise, and time-dependent velocity disturbances into the flow field and simulates a suction and blowing strip. Equations (3.11*d*), (3.11*e*) and (3.11*f*) provide the boundary conditions for the three vorticity components at the wall. Equation (3.11*d*) results from the definition of vorticity (equation (2.8)), the continuity equation (equation (2.1)), and conservation of vorticity ($\nabla\cdot\boldsymbol{\omega} = 0$). Equation (3.11*e*) results from the definition of ω_y at the wall and (3.11*f*) results from the v Poisson equation at the wall. The boundary condition for the temperature (3.11*g*) is similar to the boundary condition for the v velocity component. This condition allows for localized streamwise, spanwise, and time-dependent temperature perturbations to be introduced into the flow field.

Several comments are in order regarding boundary condition (3.11*b*) and (3.11*g*). A perturbation input into the flow field is necessary to create a forced disturbance flow. Whether the initial disturbance input into the flow is created through a suction and blowing slot or by a surface heater strip is not relevant. The functions $v_w(x,z,t)$ and $T_w(x,z,t)$ for the suction and blowing input and for the temperature input have the following forms: (*a*) Disturbance input with periodic suction and blowing:

$$v_w(x,z,t) = \begin{cases} f_v(x,z,t) & \text{if } x_B \leqslant x \leqslant x_E, \\ 0 & \text{otherwise,} \end{cases} \tag{3.12a}$$

$$T_w(x,z,t) = 0, \tag{3.12b}$$

or (*b*) Disturbance input with periodic heating:

$$v_w(x,z,t) = 0, \tag{3.13a}$$

$$T_w(x,z,t) = \begin{cases} f_T(x,z,t) & \text{if } x_B \leqslant x \leqslant x_E, \\ 0 & \text{otherwise,} \end{cases} \tag{3.13b}$$

where x_B denotes the beginning of the strip and x_E denotes the end of the strip. The generation of Tollmien–Schlichting waves was previously investigated numerically using a blowing and suction slot by Konzelmann, Rist & Fasel (1987) and a heater strip by Kral & Fasel (1991).

4. Numerical method

The numerical method of Fasel *et al.* (1990) was modified to include the energy equation and to allow for the viscosity variation with temperature. Standard central finite-difference approximations of second-order accuracy are used in the streamwise and normal directions and a spectral representation is used in the spanwise direction.

In spectral methods, the solution to a problem is represented as a truncated series of known functions for the flow variables. A continuous real function $\phi(z)$ which is periodic in the spanwise z-direction with a period of 2π; i.e., $\phi(z) = \phi(z+(2\pi/\gamma))$, can be approximated by

$$\phi(z) \simeq \sum_{k=-\frac{1}{2}K}^{k=\frac{1}{2}K} \Phi_k \, \mathrm{e}^{\mathrm{i}k\gamma z}, \tag{4.1}$$

where the Fourier coefficients Φ_k are complex conjugates

$$\Phi_{-k} = \Phi_k^*,$$

and γ is the spanwise wavenumber. The velocity, vorticity, temperature, and viscosity are assumed continuous and periodic and so are expanded in a series of the form of (4.1) where $\phi = (u, v, w, \omega_x, \omega_y, \omega_z, T, \mu)$ and $\Phi = (U, V, W, \Omega_x, \Omega_y, \Omega_z, \Theta, \mathscr{M})$.

The governing equations and boundary and initial conditions in physical space that are presented in §3 are converted to Fourier space using (4.1). This is demonstrated for two boundary conditions; further details are given in Kral (1988). Fasel *et al.* (1990) have shown that the proper choice of α^* in the outer boundary condition of (3.10*a*) is $\alpha_k^* = (\alpha_{r_M}^2 + \gamma^2 k^2)^{\frac{1}{2}}$. This condition is derived by applying the V_k Poisson equation together with the ansatz for a travelling wave from linear stability theory.

The disturbance is introduced at the wall through a suction/blowing strip or a surface heater strip. In Fourier space, the disturbance input is defined as follows: (*a*) Disturbance input with periodic suction and blowing:

for $k \leqslant 1$:

$$V_{w_k}(x, z, t) = \begin{cases} \epsilon_{V_k} \tilde{f}_{V_k}(x, t) & \text{if } x_{SB} \leqslant x \leqslant x_{SE}, \\ 0 & \text{otherwise,} \end{cases} \tag{4.2a}$$

and for $k > 1$:

$$V_{w_k}(x, z, t) = 0, \tag{4.2b}$$

for all k:

$$T_{w_k}(x, z, t) = 0, \tag{4.2c}$$

or (*b*) Disturbance input with periodic heating:

for all k:

$$V_{w_k}(x, z, t) = 0, \tag{4.3a}$$

for $k \leqslant 1$:

$$\Theta_{w_k}(x, z, t) = \begin{cases} \epsilon_{\theta_k} \tilde{f}_{\theta_k}(x, t) & \text{if } x_{HB} \leqslant x \leqslant x_{HE}, \\ 0 & \text{otherwise,} \end{cases} \tag{4.3b}$$

and for $k > 1$:

$$\Theta_{w_k}(x, z, t) = 0. \tag{4.3c}$$

The functions $f_v(x, z, t)$ and $f_T(x, z, t)$ are chosen to be of the following form:

$$f_v(x, z, t) = \tilde{f}_v(x, t)(\epsilon_{v_0} + \epsilon_{v_1} \cos \gamma z), \tag{4.4a}$$

$$f_T(x, z, t) = \tilde{f}_T(x, t)(\epsilon_{T_0} + \epsilon_{T_1} \cos \gamma z). \tag{4.4b}$$

The parameters ϵ_{v_0}, ϵ_{v_1}, ϵ_{T_0}, and ϵ_{T_1} determine the two-dimensional and three-dimensional input amplitudes.

With the use of the spectral ansatz in the spanwise direction, the three-dimensional governing equation system reduces to $3K$ vorticity transport equations, $3K$ Poisson equations for the velocities, K energy equations, and K viscosity equations, where K is the number of Fourier modes retained in the spectral approximation. The resulting two-dimensional system of equations is solved in Fourier space. The vorticity transport and energy equations are advanced in time using backward differences of second-order accuracy. Owing to the elliptic nature with respect to x and y of the governing equations, a large system of equations has to be solved. These equations systems are solved using a Gauss–Seidel line relaxation procedure. The nonlinear terms are updated throughout the iterative procedure with the iterations continuing until convergence is achieved. For details of the numerical method, see Kral (1988).

5. Results

The numerical method was first tested extensively with calculations of two- and three-dimensional waves of very small amplitudes. Detailed comparison with linear stability theory and experiments was made to provide a thorough check of the numerical method. The method was then applied to simulate control of the nonlinear secondary instability process for both the fundamental and subharmonic breakdown processes.

5.1. *Passive control of linear disturbances using uniform wall heating*

The parameters chosen for the simulation of control of linear disturbances closely model the experiments of Strazisar, Reshotko & Prahl (1977) and Strazisar & Reshotko (1978). Although only control of two-dimensional waves was considered in these experiments, here the control of small-amplitude three-dimensional oblique waves is investigated in addition to the two-dimensional waves.

The fluid in the physical experiments was water which was therefore used for all the control investigations reported here. The free-stream temperature $\bar{T}_\infty$ in the experimental investigations was 75 °F (or 23.89 °C). For water at this temperature, the dynamic viscosity $\bar{\mu}_\infty$ is 9.135×10^{-4} kg m s^{-1} and the Prandtl number Pr is 6.3. A Reynolds number Re of 1×10^5 was used with a free-stream velocity $\bar{U}_\infty$ of 3 m s^{-1} and a reference length $\bar{L}$ of 0.0353 m. Results of control of a disturbed flow forced with frequency $F = 1$ (F is the non-dimensional frequency parameter, defined as $F = \bar{\beta}\bar{\nu}_\infty 10^4/\bar{U}_\infty^2$ where $\bar{\beta}$ is the dimensional circular frequency) will be discussed in detail and comparison with experiments will be made at both $F = 1$ and $F = 1.55$. For the case with $F = 1$, ($\beta = 10$), the following parameters were used: Re_{δ_1} (at x_0) = 500, $\gamma = 20$, and $K = 2$. For the case with $F = 1.55$, ($\beta = 15.5$), the parameters were: Re_{δ_1} (at x_0) = 475, $\gamma = 20$, and $K = 2$. The same spanwise wavenumber γ was chosen for both frequencies. Thus, for $F = 1$, the oblique waves are at an angle of about 35° with respect to the x-axis and for $F = 1.55$, the oblique angle is approximately 26° with

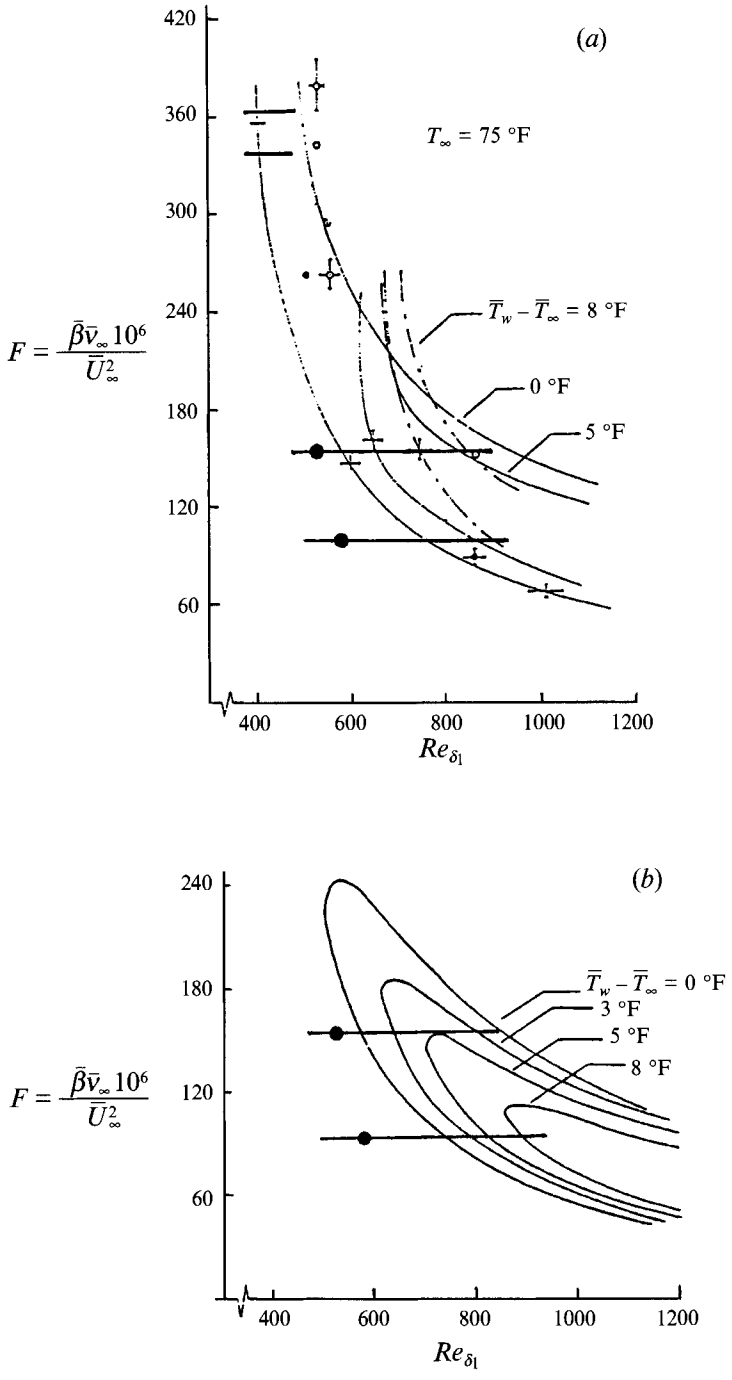

FIGURE 2. Stability diagram for a uniformly heated wall from (*a*) experiments of Strazisar *et al.* (1977) and (*b*) linear stability theory of Lowell (1974). Solution domain for Navier–Stokes calculations of small-amplitude disturbances is shown by the horizontal bars with the location of the disturbance input shown by ●.

respect to the x-axis. In the calculations, approximately 30 grid points per disturbance wavelength were used and the solution domain contained approximately 16 disturbance wavelengths. One time period was discretized with 60 time intervals. The y-direction spanned approximately ten boundary-layer displacement thicknesses at the inflow boundary and about five boundary-layer displacement thicknesses at the outflow boundary. The x extent of the computational domain in relation to the linear stability theory diagram is shown in figure 2 for both frequencies. The stability diagram in figure 2(*a*) is from the experimental investigation by Strazisar *et al.* (1977) and the stability diagram of figure 2(*b*) is from the linear stability theory calculations by Lowell (1974). The stabilizing effect of uniform heating can be observed for both stability diagrams where neutral curves are shown for different levels of wall heating. Significant differences exist between measurements and theory at the higher frequencies. Strazisar *et al.* (1977) attributed non-parallel effects to the crossing of the neutral curves (in figure 2*a*). However, this phenomena cannot be observed in parallel linear stability analysis.

For the control simulations of linear disturbances, the perturbations are introduced through periodic heating at the wall simulating a flush mounted heater strip as used in the experiments by Liepmann *et al.* (1982). The wall boundary conditions for the undisturbed flow follow from (4.3):

$$\hat{\Theta}_{x_n, y=0} = A_0 x_n^p + \sin^2(\xi_n). \tag{5.1a}$$

The wall boundary conditions for the disturbed flow for $k \leqslant 1$ are:

$$\Theta_{x_n, y=0, z_k} = \sin^2(\xi_n)[\epsilon_{\Theta_k} \sin(\beta_k t)], \tag{5.1b}$$

where

$$\xi_n = \frac{x_n - x_{HB}}{x_{HE} - x_{HB}} \pi,$$

and

$$x_{HB} \leqslant x_n \leqslant x_{HE}.$$

The heater strip is located one disturbance wavelength downstream of the left boundary ($x_{HB} = 30$ and $x_{HE} = 45$) and its width is about half of a Tollmien–Schlichting wavelength. The location of the heater strip relative to the neutral curves is also shown in figure 2. The width of the heater strip and streamwise shape function are chosen based on a receptivity study of a surface heater strip. Details of the study can be found in Kral & Fasel (1991). The disturbance amplitudes ϵ_{Θ_0} and ϵ_{Θ_1} are chosen so that the temperature perturbations create linear disturbance velocities with a maximum of approximately 0.05% of the free-stream velocity. The x-distribution is chosen so that the temperature input from the heater strip represents heating only and no cooling. For the present calculations, the temperature inputs to the heater strip were 1.1 °F (2 °C) for the oscillatory component and 1.67 °F (3 °C) for the mean component.

Before presenting results of the control simulations, the calculation of linear disturbance waves without control is discussed. The uncontrolled flow simulations form a basis for comparison with the controlled simulations. In addition, comparison with linear stability theory provides validation of the code. Mean flow quantities were compared and the growth of the boundary-layer displacement thickness and skin friction are nearly identical for the Navier–Stokes and the Blasius similarity solutions.

The disturbance flow resulting from the time periodic disturbance input at the heater strip is shown in figure 3 for the streamwise velocity component. Shown are perspective representations of each Fourier mode which were obtained after nine periods had been computed. The two-dimensional mode ($k = 0$) is shown in figure 3(*a*). The three-dimensional mode ($k = 1$) is shown in figure 3(*b*) for the three-dimensional oblique wave. The disturbance waves decay at first and then begin to amplify downstream. This

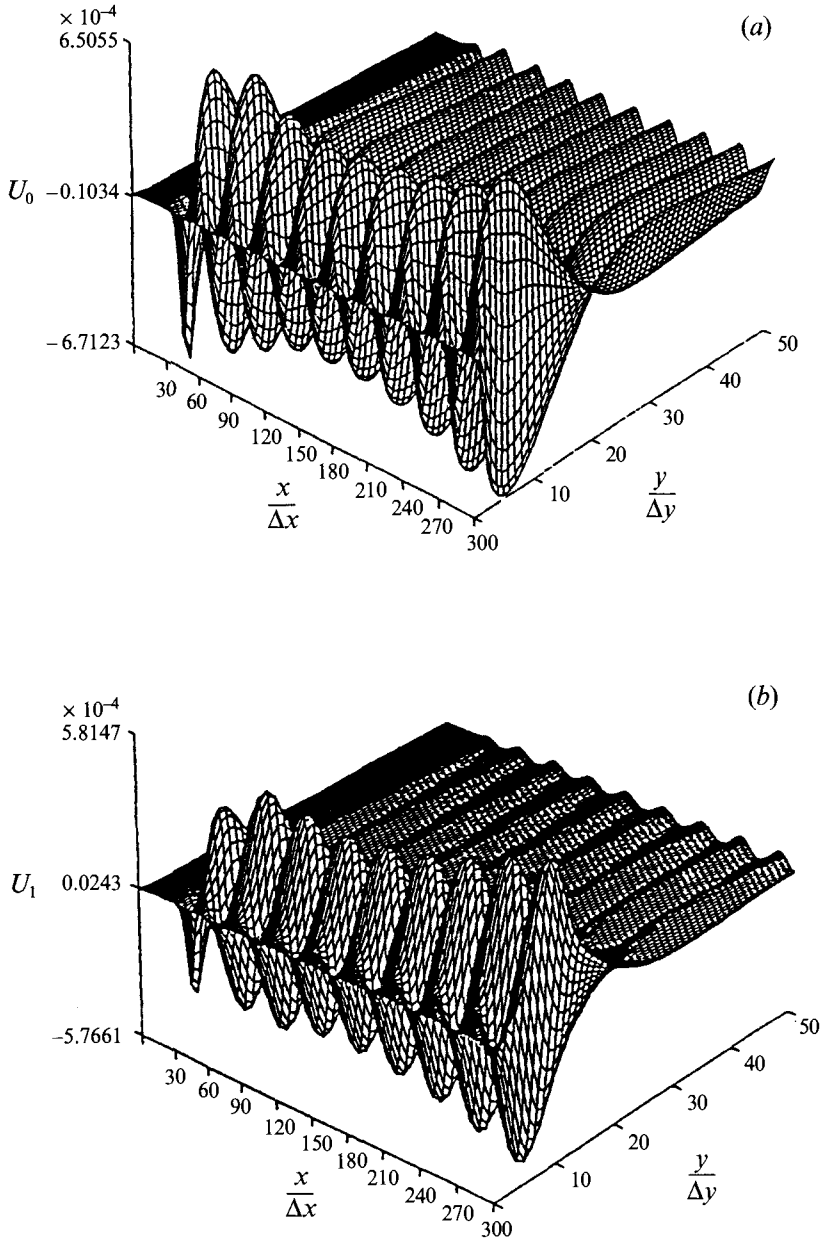

FIGURE 3. Uncontrolled instantaneous, disturbed flow after nine periods of oscillation at $F = 1$ for the (*a*) two-dimensional streamwise velocity component, U_0 and (*b*) three-dimensional streamwise velocity component, U_1.

behaviour is in qualitative agreement with the stability diagram of figure 2 in which, for the two-dimensional disturbances, the calculation begins in the stable region and then crosses the neutral curve into the region of instability. Although the stability diagram is for two-dimensional disturbances, the three-dimensional growth is similar to the two-dimensional growth for this chosen oblique angle.

The computations for small-amplitude perturbations should be comparable to the Orr–Sommerfeld solution. To allow comparison, we have solved the Orr–Sommerfeld

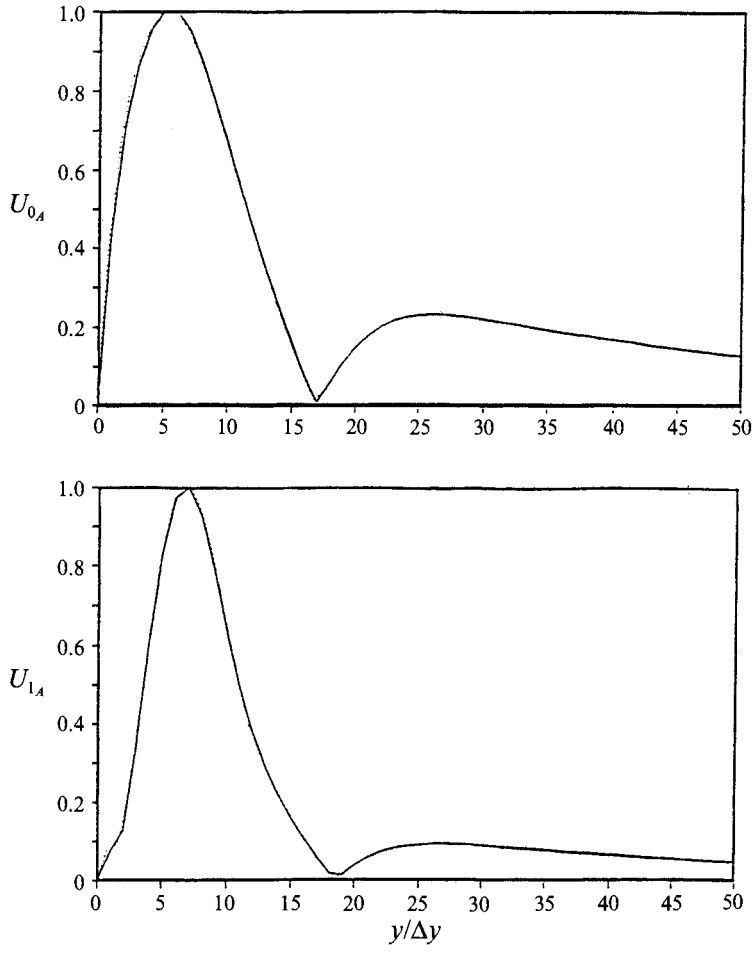

FIGURE 4. Comparison of amplitudes between ——, the Navier–Stokes solution and ·····, linear stability theory without control applied for $F = 1$ at $Re_{\delta_1} = 800$ for the (*a*) two-dimensional streamwise velocity, U_0 and (*b*) three-dimensional streamwise velocity, U_1.

equation for both two-dimensional waves and three-dimensional oblique waves. The linear stability theory solution is compared with the Navier–Stokes solution at a displacement thickness Reynolds number $Re_{\delta_1} = 800$ ($n = 175$). Amplitude profiles are obtained from the Navier–Stokes calculations by a Fourier time series analysis over one period of oscillation. The Navier–Stokes solution is normalized with the linear stability theory calculation by the maximum of the U_k disturbance velocity. Figure 4 displays the exceptional agreement in amplitudes of the streamwise velocity for both mode 0 and mode 1. Similar agreement with linear stability theory for a calculation with frequency $F = 1.55$ is shown in Kral (1988).

For each frequency, control using a uniform surface temperature distribution was investigated for four cases, three of which had uniform heating and one had uniform cooling applied at the wall. For this, the parameter p in (5.1) was set to 0 since the surface temperature distribution is uniform at the wall. The levels of heating (set in (5.1)) for the four cases were: $\Delta\bar{T} = 3$ °F, $\Delta\bar{T} = 5$ °F, $\Delta\bar{T} = 8$ °F, and $\Delta\bar{T} = -5$ °F.

Results of a disturbed flow for a uniformly heated wall with $\Delta\bar{T} = 8$ °F and $F = 1$ are shown in figure 5. Perspective representations of each Fourier mode for the streamwise velocity are shown after nine time periods. For both the two- and three-dimensional

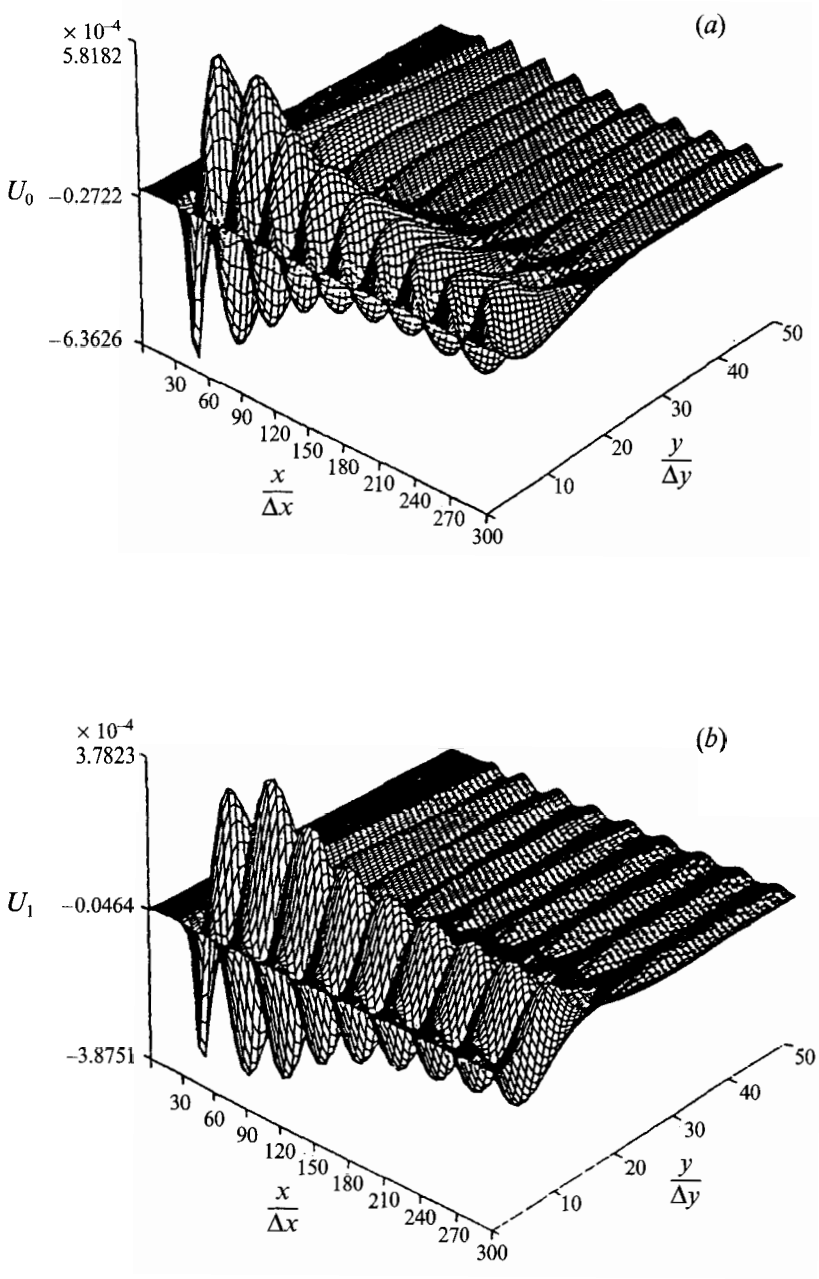

FIGURE 5. Instantaneous, disturbed flow after nine periods of oscillation at $F = 1$ with $\Delta\bar{T} = 8\ °\mathrm{F}$ uniform wall heating applied for the (*a*) two-dimensional streamwise velocity, U_0, and (*b*) three-dimensional streamwise velocity, U_1.

components, the influence of the uniform control on the disturbed flow is obvious. The flow components show a strong damping downstream of the disturbance input. The behaviour of the two-dimensional waves is in qualitative agreement with the linear stability diagram of figure 2(*b*) for $\Delta\bar{T} = 8\ °\mathrm{F}$ in which decay is expected for the computational domain used.

To illustrate the effects of heating for all four cases, amplitude profiles are shown in figure 6 for the streamwise velocity and the streamwise vorticity. The comparison is

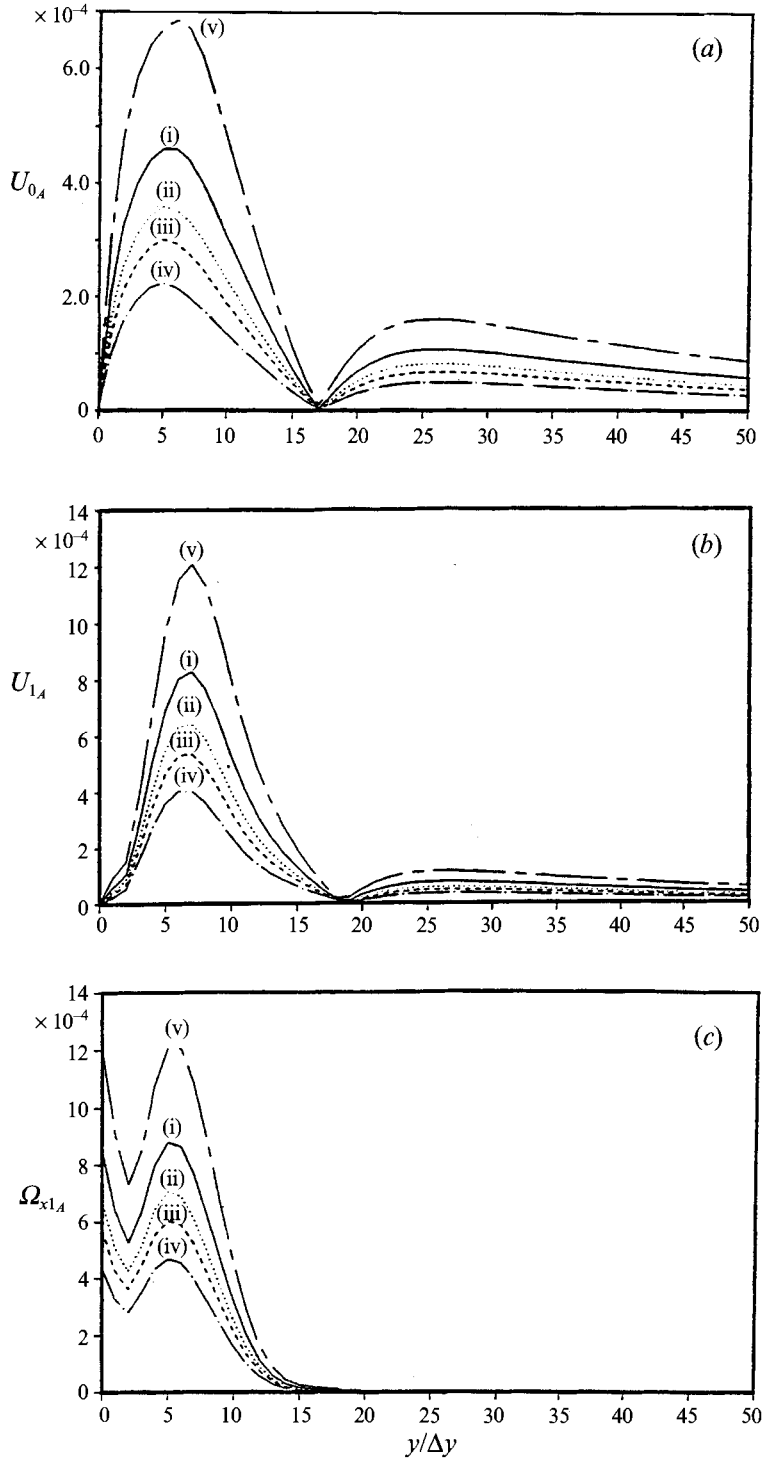

FIGURE 6. Amplitude profiles for varying levels of wall heating at $Re_{\delta_1} = 800$ and $F = 1$ for the (*a*) two-dimensional streamwise velocity, U_0, (*b*) three-dimensional streamwise velocity, U_1, and (*c*) three-dimensional streamwise vorticity, Ω_{x_1}. (i) $\Delta\bar{T} = 0$ °F, (ii) 3 °F, (iii) 5 °F, (iv) 8 °F, (v) −5 °F.

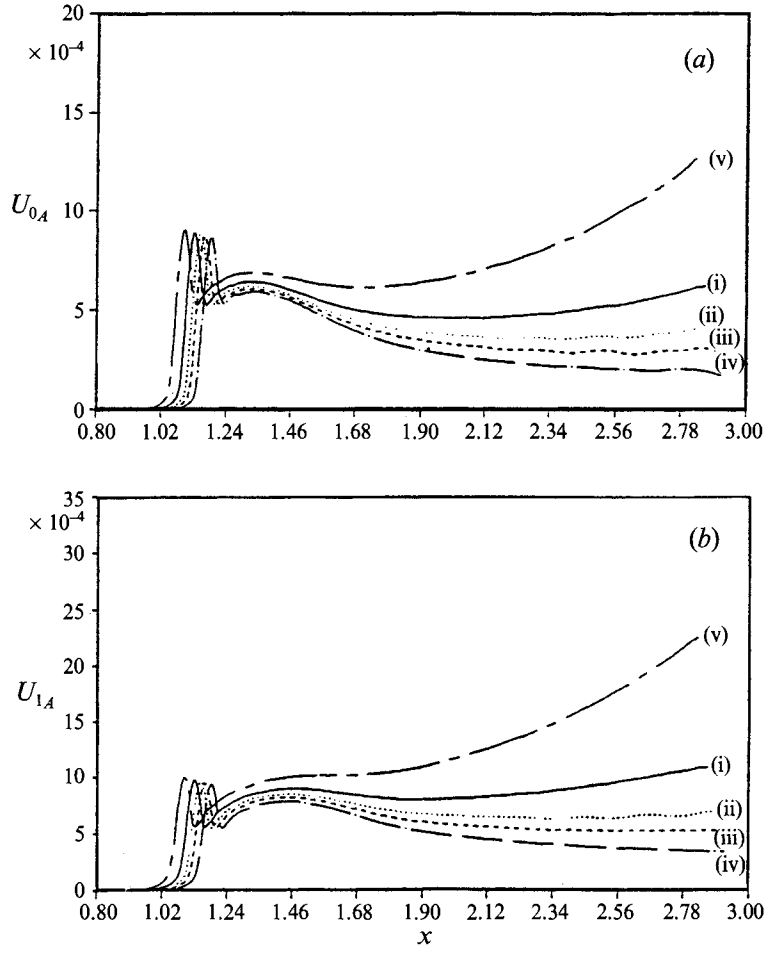

FIGURE 7. Influence of uniform wall heating on the amplitude growth at $F = 1$ for the (a) inner maximum of the two-dimensional streamwise velocity, U_0 and (b) inner maximum of the three-dimensional streamwise velocity, U_1. (i) $\Delta\bar{T} = 0$ °F, (ii) 3 °F, (iii) 5 °F, (iv) 8 °F, (v) −5 °F.

made at a displacement thickness Reynolds number of $Re_{\delta_1} = 800$. With each incremental increase in heating, the amplitude levels are reduced for the velocity and vorticity, while wall cooling results in an increase in amplitudes. The shape of the amplitudes does not change significantly.

In connection with the reduction in amplitude levels, the growth rates are also affected. The downstream growth of the amplitude is shown in figure 7 for all cases. The amplitudes at the maximum of the U_0 and U_1 disturbance velocity components are plotted versus the streamwise x-direction. The reduction in amplitudes with increasing uniform wall heating can be seen for both the two- and three-dimensional components. In contrast, cooling increases the amplitudes.

In the following, a direct comparison of the growth rates obtained from the Navier–Stokes calculations with those from stability theory and experiments is made for both $F = 1$ and $F = 1.55$ with uniform heating applied. The growth rate α_i is calculated from the Navier–Stokes solution by $\alpha_{i_0} = -\mathrm{d}(\ln(A_0/A_{ref}))/\mathrm{d}x$ where A_0 represents the two-dimensional amplitude of the flow variable upon which the stability criterion is based and A_{ref} is a reference amplitude. Here, only the linear two-

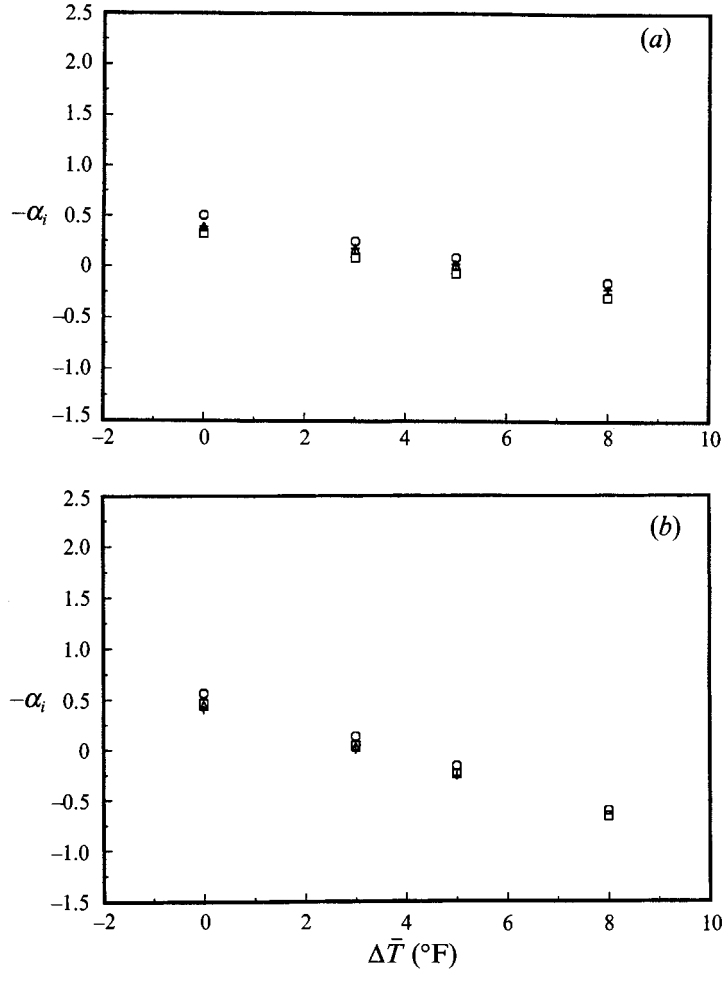

FIGURE 8. Comparison of amplification rates from Navier–Stokes calculations with parallel linear stability theory for uniform wall heating at $Re_{\delta_1} = 800$ for (*a*) $F = 1$ and (*b*) $F = 1.55$. □, Navier–Stokes (inner max u); ○, Navier–Stokes (max v); △, parallel theory (Lowell); +, parallel theory (El-Hady *et al.*).

dimensional amplification rates are compared since the experimental and theoretical work was for two-dimensional Tollmien–Schlichting waves only. Figure 8(*a*) shows a comparison of the Navier–Stokes results with parallel linear stability theory for different heating levels at $Re_{\delta_1} = 800$ for $F = 1$ and figure 8(*b*) shows a comparison at $Re_{\delta_1} = 800$ for $F = 1.55$. The amplification rates from the numerical simulations were calculated at the inner maximum of the U_0 velocity and at the maximum of the V_0 velocity. Shown for comparison are the linear stability theory results of Lowell (1974) and El-Hady & Nayfeh (1979) for a parallel uniformly heated boundary layer. Although El-Hady & Nayfeh also performed a non-parallel stability analysis for the heated flow, the streamwise distortion of the eigenfunctions of the disturbances was neglected for these particular cases. El-Hady (1990, private communication) claims that this distortion must be taken into account for an accurate non-parallel analysis and so comparison is made only with the parallel theory.

The linear stability theory results of Lowell and El-Hady & Nayfeh agree well for the cases shown. (Lowell also predicts a damping, in agreement with the Navier–Stokes

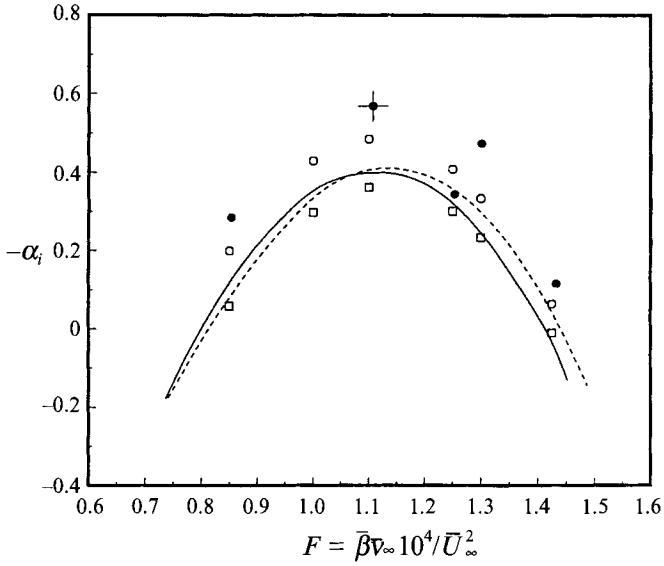

FIGURE 9. Comparison of amplification rates from Navier–Stokes calculations with linear stability theory and experiment for $\Delta\bar{T} = 3.48$ °F and $Re_{\delta_1} = 863$. □, Navier–Stokes (inner max u); ○, Navier–Stokes (max v); +, parallel (El-Hady *et al.*); ——, non-parallel (inner max u) (El-Hady *et al.*); ●, experiments (inner max u) (Strazisar *et al.*).

solutions, for $\Delta\bar{T} = 8$ °F at $F = 1$ and for $\Delta\bar{T} = 5$ °F and $\Delta\bar{T} = 8$ °F at $F = 1.55$, but the exact growth rates were unavailable.) The growth rates obtained from the Navier–Stokes calculations for the V_0 velocity component are higher than the growth rates obtained from linear stability theory. Based on the U_0 velocity at $F = 1.0$, the Navier–Stokes solution predicts a slightly lower growth rate than linear stability theory, but the agreement is quite good between the Navier–Stokes calculations and linear stability theory for the U_0 velocity component at $F = 1.55$. As the level of heating is increased, the difference between the growth rate based on the U_0 velocity component and the V_0 velocity component is diminishing. In the linear stability theory calculations, all fluid properties may vary with temperature. However, Lowell's results showed no appreciable differences for even larger levels of heating with the linear stability calculations of Wazzan *et al.* (1968, 1970*a*, *b*) in which only the viscosity variation with temperature for the base flow was considered. The slight differences between the Navier–Stokes solutions with linear stability theory could also be attributed to the different property relationships used in the Navier–Stokes calculations and the stability investigations.

The neutral curves, obtained from the measurements by Strazisar *et al.* (1977) (see figure 2*a*), are based on the inner maximum of the U_0 velocity component. One would conjecture that the amplification rates decrease with increasing heating for $\Delta\bar{T} = 3$ °F and $\Delta\bar{T} = 5$ °F at $F = 1.55$, however, the amplification rates show a slight increase for $\Delta\bar{T} = 8$ °F. This same trend is not predicted by the linear stability theory of Lowell or El-Hady & Nayfeh or by our numerical simulations which allow for all non-parallel effects. The non-parallel effects alluded to in the experimental investigations that caused the neutral curves to overlap are not seen in this work.

Comparison with the parallel and non-parallel theory by El-Hady & Nayfeh and the experiments by Strazisar *et al.* is shown in figure 9 for $\Delta\bar{T} = 3.48$ °F and $Re_{\delta_1} = 863$. In the non-parallel analysis, the growth rates are based on the inner maximum of the U_0

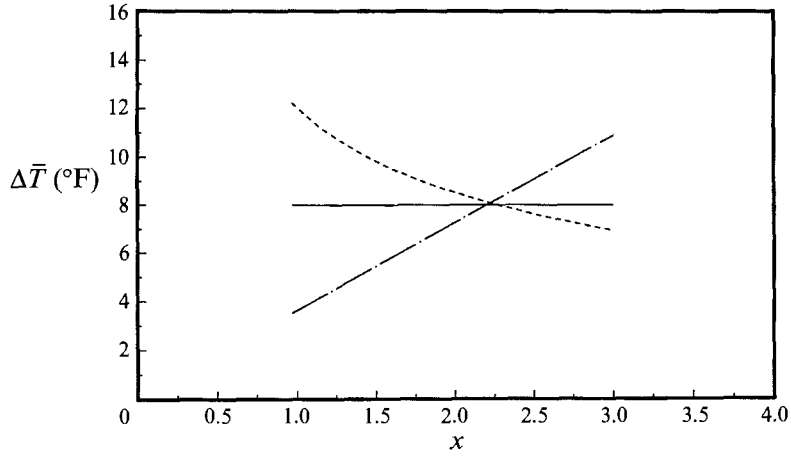

FIGURE 10. Power law temperature distributions for $\Delta\bar{T} = A_0 x_n^p = 8$ °F at $Re_{\delta_1} = 800$ and (*a*) $F = 1$ and (*b*) $F = 1.55$. ——, $p = 0$; – – –, 0.5; —·—, 1.0.

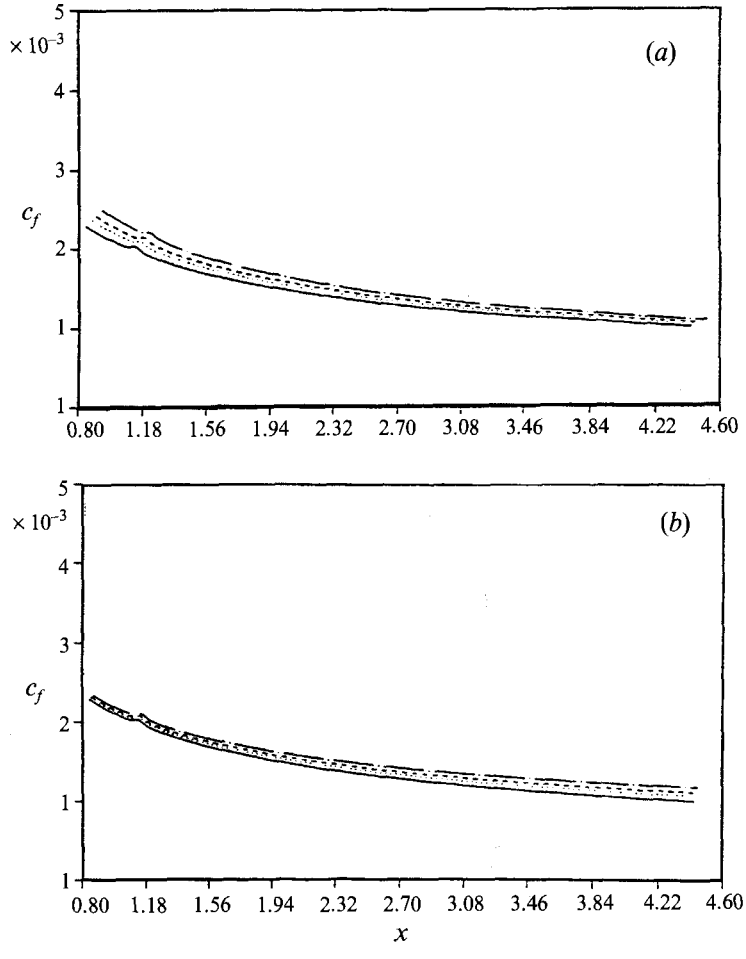

FIGURE 11. Influence of non-uniform wall heating on the skin friction ($F = 1$) for (*a*) $\Delta\bar{T} = A_0 x_n^{-0.5}$ and (*b*) $\Delta\bar{T} = A_0 x_n^{1.0}$. ——, $\Delta\bar{T} = 0$ °F; ..., $\Delta\bar{T}(Re_{\delta_1} = 800) = 3$ °F' – – –, $\Delta\bar{T}(Re_{\delta_1} = 800) = 5$ °F; —·—, $\Delta\bar{T}(Re_{\delta_1} = 800) = 8$ °F.

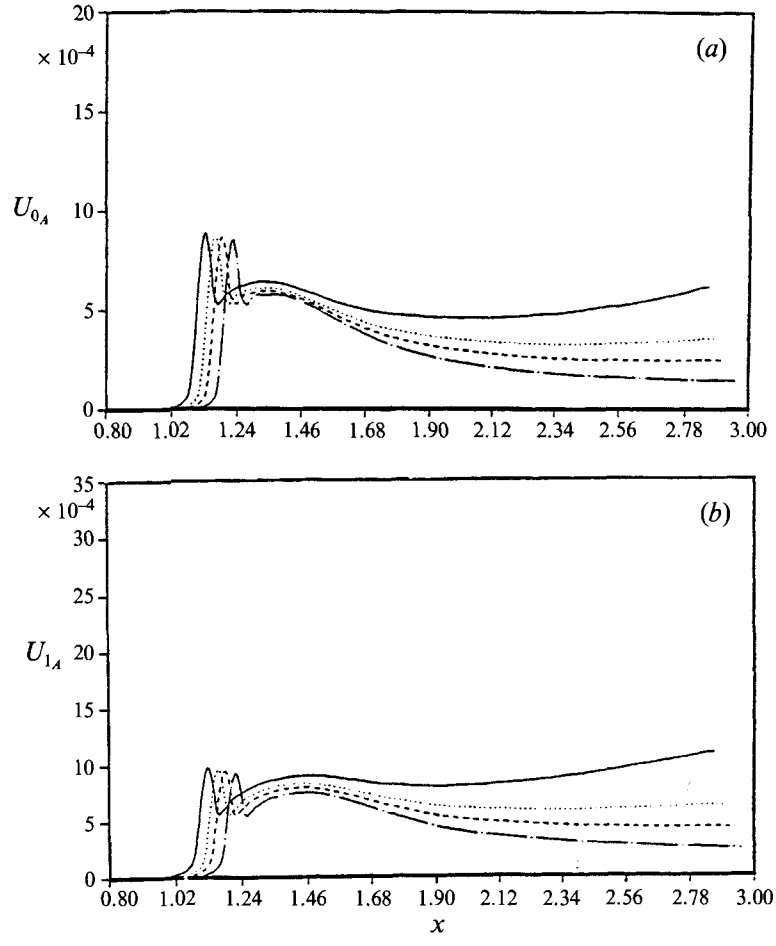

FIGURE 12. Influence of non-uniform heating on the amplitude growth for $A_0 x_n^{-0.5}$, $F = 1$, based on (*a*) the inner maximum of the two-dimensional streamwise velocity, U_0 and (*b*) the second inner maximum of the three-dimensional streamwise velocity, U_1. See figure 11 for key.

velocity and the distortion of the U_0 eigenfunction with streamwise position is included in the definition of the growth rates. The amplification rates based on the inner maximum of the U_0 velocity and the maximum of the V_0 velocity obtained from the direct simulations are also shown. The higher growth rates based on the V_0 velocity component instead of the U_0 velocity component are consistent with the results obtained from non-parallel investigations for the unheated case (Fasel & Konzelmann 1990). The growth rates obtained from the Navier–Stokes simulation based on the U_0 velocity agree better with the non-parallel theory at the lower frequencies. The non-parallel theory predicts slightly larger growth rates at the higher frequencies when compared with the growth rates from the direct simulations. The experimental data (also based on the inner maximum of the U_0 velocity) predict larger growth rates than parallel and non-parallel theory and the direct simulations for this level of heating. The discrepancy between the experiments and the full simulations cannot be due to non-parallel effects since these effects are included in our numerical model.

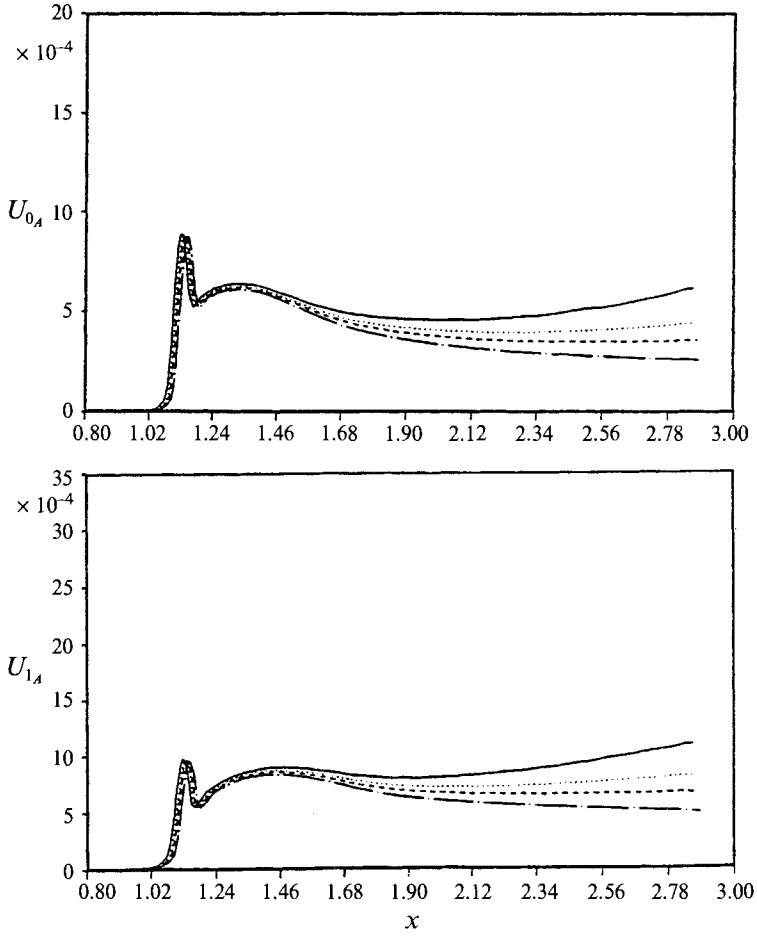

FIGURE 13. Influence of non-uniform heating on the amplitude growth for $A_0 x_n^{1.0}$, $F = 1$, based on (*a*) the inner maximum of the two-dimensional streamwise velocity, U_0 and (*b*) the second inner maximum of the three-dimensional streamwise velocity, U_1. See figure 11 for key.

5.2. *Passive control of linear disturbances using non-uniform wall heating*

As shown previously, uniform wall heating enhances stability. However, a non-uniform wall temperature distribution may lead to even stronger stabilization of the flow and may require less heat input than for uniform heating. To confirm this, two different non-uniform temperature distributions of the power law form $A_0 x_n^p$ were used for both frequencies $F = 1$ and $F = 1.55$. The two exponents used were $p = -0.5$ and $p = 1.0$. The following cases of non-uniform heating were considered: $\Delta\bar{T} = 3$ °F, $\Delta\bar{T} = 5$ °F, and $\Delta\bar{T} = 8$ °F. The parameters were chosen to simulate the experiments of Strazisar & Reshotko (1978). Comparison of these two non-uniform surface heating distributions will be made with the experiments of Strazisar & Reshotko and the stability theory of Nayfeh & El-Hady (1980). In the experiments, the wall temperature is held fixed at a reference location x_r corresponding to a Reynolds number $Re_{\delta_1}(x_r) = 800$ for the unheated case. In the numerical simulations, the temperature is held constant at this Reynolds number at the above prescribed heating level. The power law temperature distributions are shown in figure 10 for the case of $\Delta\bar{T} = 8$ °F at $Re_{\delta_1} = 800$. For $p = -0.5$, the temperature difference is larger than for the uniform

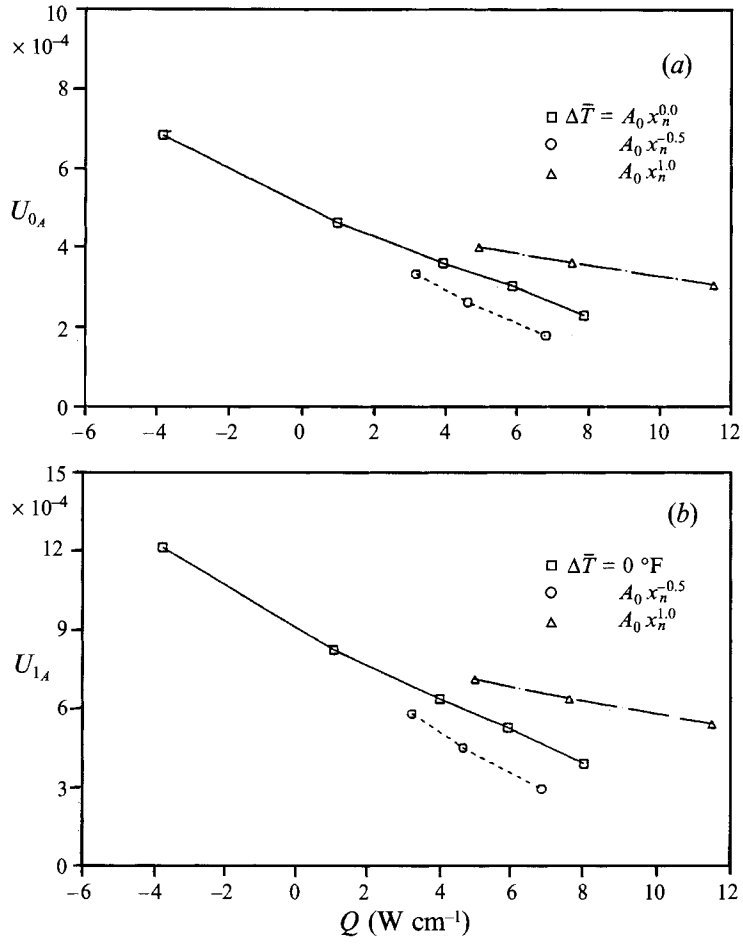

FIGURE 14. Comparison of wall heat input and level of control achieved, $F = 1$ and $Re_{\delta_1} = 800$ based on the amplitude at (*a*) the inner maximum of the two-dimensional streamwise velocity, U_0 and (*b*) the second inner maximum of the three-dimensional streamwise velocity, U_1.

heating case at all locations upstream of $Re_{\delta_1} = 800$ ($x_r \approx 2.2$), while the temperature difference is below the uniformly heated case for $p = 1.0$. Downstream of $Re_{\delta_1} = 800$, the temperature difference decreases below the uniformly heated level for $p = -0.5$, but increases for $p = 1.0$. For an increased temperature difference, the velocity profile $\partial\hat{u}/\partial y$ is fuller, thus enhancing stability. Therefore, the non-uniform wall heating case of $A_0 x_n^{-0.5}$ should provide a more stabilizing influence than $A_0 x_n^{1.0}$ and $A_0 x_n^{0.0}$ upstream of $Re_{\delta_1} = 800$, while $A_0 x_n^{1.0}$ is more stabilizing downstream of the reference location. This is an important point when comparing different non-parallel surface temperature distributions, and has been discussed by Asrar & Nayfeh (1985).

For the non-uniform surface temperature distributions used in this work, the reference point is located towards the end of the computational domain. Therefore, it is expected that the exponent $p = -0.5$ is more stabilizing than $p = 1.0$ and $p = 0$.

Results of non-uniform surface heating for the frequency $F = 1$ are shown in detail. At the beginning of the streamwise domain, the skin friction, shown in figure 11, is larger for $p = -0.5$ than for $p = 1.0$, while the opposite occurs further downstream. The larger skin friction means a fuller base flow velocity profile and thus enhanced stability.

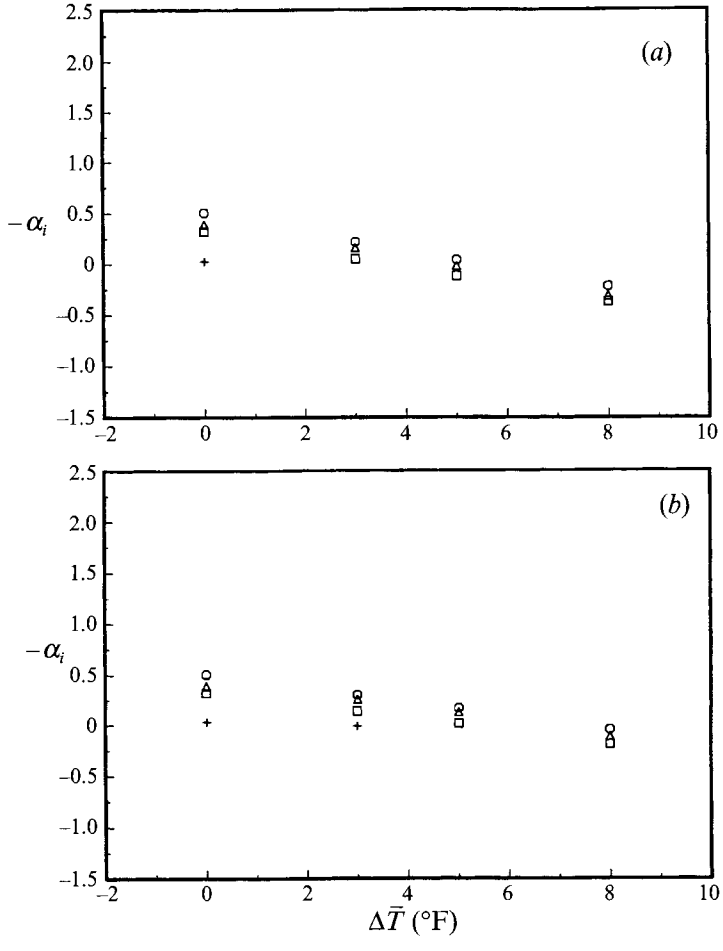

FIGURE 15. Comparison of amplification rates from Navier–Stokes calculations with parallel linear stability theory and experiments for non-uniform wall heating at $Re_{\delta_1} = 800$, $F = 1$ for (*a*) $A_0 x_n^{-0.5}$ and (*b*) $A_0 x_n^{1.0}$. □, Navier–Stokes (inner max u); ○, Navier–Stokes (max v); △, parallel (inner max u) (El-Hady *et al.*): +, experiments (inner max u) (Strazisar *et al.*).

The downstream growth of the amplitudes, for the maximum of the U_0 and U_1 velocities is shown in figures 12 and 13 for both $p = -0.5$ and $p = 1.0$. Here it is obvious that the stabilizing influence is more pronounced for $p = -0.5$ then for $p = 1.0$.

In order to compare accurately the efficiency of control using non-uniform temperature heating with that of uniform temperature heating, the actual heat input to the wall is compared in figure 14. The amplitude at the maximum of the U_k velocity at $Re_{\delta_1} = 800$ versus the heat input over the computational domain is shown for each heating case considered. Both the two- and three-dimensional modes are shown. The actual heat input required for the same reduction in amplitude is lower for $p = -0.5$ than for $p = 0$ and $p = 1.0$. This makes the temperature distribution $A_0 x_n^{-0.5}$ the most energy efficient one of the distributions considered when the reference location is near the end of the controlled flow field. The temperature distribution $A_0 x_n^{1.0}$ should be more efficient if the reference location is near the beginning of the control region.

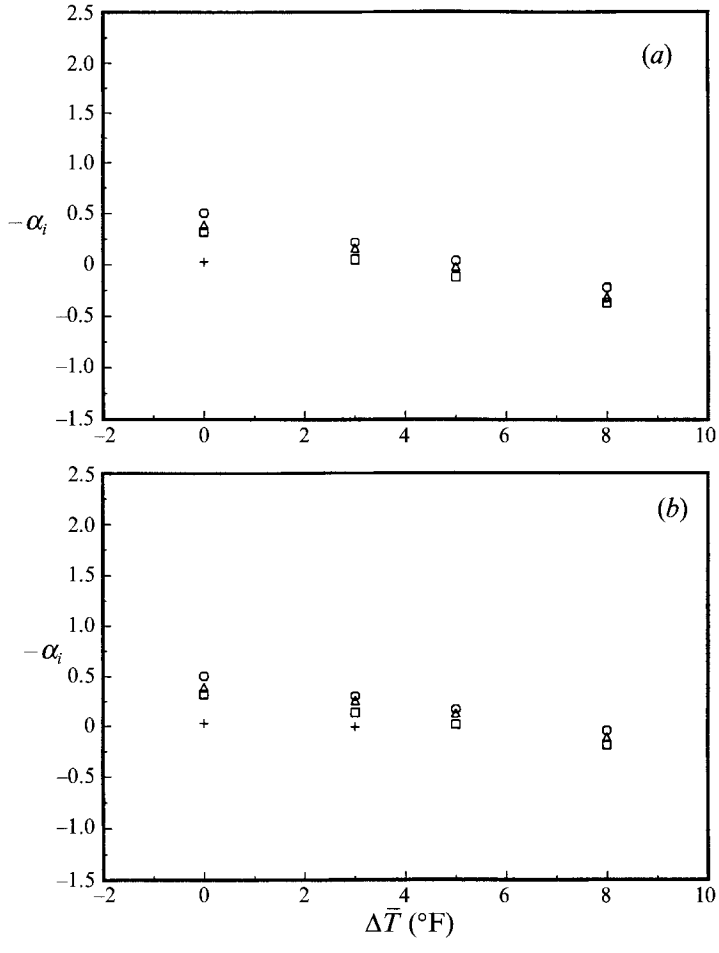

FIGURE 16. Comparison of amplification rates from Navier–Stokes calculations with parallel linear stability theory and experiments for non-uniform wall heating at $Re_{\delta_1} = 800$, $F = 1.55$ for (*a*) $A_0 x_n^{-0.5}$ and (*b*) $A_0 x_n^{1.0}$. See figure 15 for key.

Comparison with theory and experiments for non-uniform surface heating is made for both $F = 1$ and $F = 1.55$. As before, only the linear two-dimensional amplification rates are compared since the experimental and theoretical work was for two-dimensional waves. Figures 15 and 16 show a comparison of the amplification rates at $Re_{\delta_1} = 800$ for different levels of heating. In figures 15(*a*) and 16(*a*), the temperature distribution applied at the wall is $A_0 x_n^{-0.5}$ and in figures 15(*b*) and 16(*b*) the temperature distribution is $A_0 x_n^{1.0}$. The linear stability theory results of Nayfeh & El-Hady (1980) for a parallel, non-uniformly heated boundary layer are shown. (Again, the comparison with the non-parallel results is not made since the streamwise distortion of the eigenfunction was not taken into account in the stability analysis.) In addition, the amplification rates from the experimental work of Strazisar & Reshotko (1978) are compared where available. The experimental points are deduced from curves faired through the measurements near $Re_{\delta_1} = 800$.

As was the case for uniform heating, the agreement in the growth rates between parallel linear theory and the full simulations is better when based on the inner maximum of the U_0 velocity than the maximum V_0 velocity. The discrete values of the

growth rates from the experiments are not available for all cases considered, but the trends showed good qualitative agreement with the numerical simulations. For $F = 1$ and $p = -0.5$, both the direct simulations and the experiments showed a damping. For $F = 1$ and $p = 1.0$, the experimental points indicate a stabilized boundary layer, also in agreement with the Navier–Stokes calculations.

For $p = -0.5$ and $F = 1.55$, the trend towards stabilization for higher levels of heat input is found in the experiments. However, for $p = 1.0$, the experimental growth rate increases for $A_0 x_n^{1.0} = 3$ °F and then decreases for $A_0 x_n^{1.0} = 5$ °F. The growth rate for $A_0 x_n^{1.0} = 8$ °F from the experimental work shows a damped value. The increase and decrease in growth rates was also seen in the experiments of Strazisar *et al.* (1977) for uniform heating at $F = 1.55$. This trend is again not seen in either the full Navier–Stokes simulations or the stability analysis.

5.3. *Passive control of secondary instability using uniform wall heating*

In addition to control of small-amplitude two- and three-dimensional disturbances, control of the early stages of the nonlinear three-dimensional secondary instability process was also investigated. For this, uniform heating was applied for both the fundamental ordered peak–valley and the subharmonic staggered breakdown processes. The parameters chosen for the simulation of secondary instability closely model the experiments of Klebanoff *et al.* (1962) for the fundamental breakdown and Kachanov & Levchenko (1984) for the subharmonic breakdown. However, boundary-layer control was not applied in these experimental investigations. Unfortunately, neither theoretical nor experimental investigations with control of the spatial secondary instability process are available. Therefore, the above experiments only provide a qualitative reference for comparison of the influence of passive heating on the secondary instability process.

Values for several parameters were the same as for the simulations discussed previously, including $\bar{T}_\infty$, $\bar{\mu}_\infty$, Pr, Re, $\bar{U}_\infty$, and $\bar{L}$. The remaining parameters differ for the two different secondary instability processes. First, the results for control of fundamental breakdown are discussed, followed by the results for control of the subharmonic breakdown process.

5.3.1. *Passive control of the fundamental breakdown process*

The parameters used in the investigation of control of the ordered peak–valley breakdown process were: $F_{2D} = 0.588$ ($\beta_{2D} = 5.88$), $F_{3D} = 0.588$ ($\beta_{3D} = 5.88$), $\gamma = 24.3$, $K = 2$, $\epsilon_{V_0} = 1.2 \times 10^{-3}$, and $\epsilon_{V_1} = 2.4 \times 10^{-4}$. The frequencies for both the two- and three-dimensional disturbance input are the same. These parameters are chosen to match as closely as possible the conditions of the experiments of Klebanoff *et al.* (1962). Approximately 60 grid points per disturbance wavelength are used and the streamwise domain contains about 15 disturbance wavelengths. The y-direction spans 5.5 boundary-layer displacement thicknesses at the inflow boundary and approximately five boundary-layer displacement thicknesses at the outflow boundary. There are 100 timesteps per disturbance period. The computation proceeds for eight disturbance periods. Numerical tests have shown that, in the region considered, two Fourier modes are sufficient to resolve the spanwise flow.

For all control simulations of secondary instability, the disturbances are introduced through periodic blowing and suction by a narrow strip at the wall. The wall boundary conditions follow from (4.2) for the undisturbed flow:

$$\hat{\Theta}_{x_n, y=0} = A_0, \tag{5.2a}$$

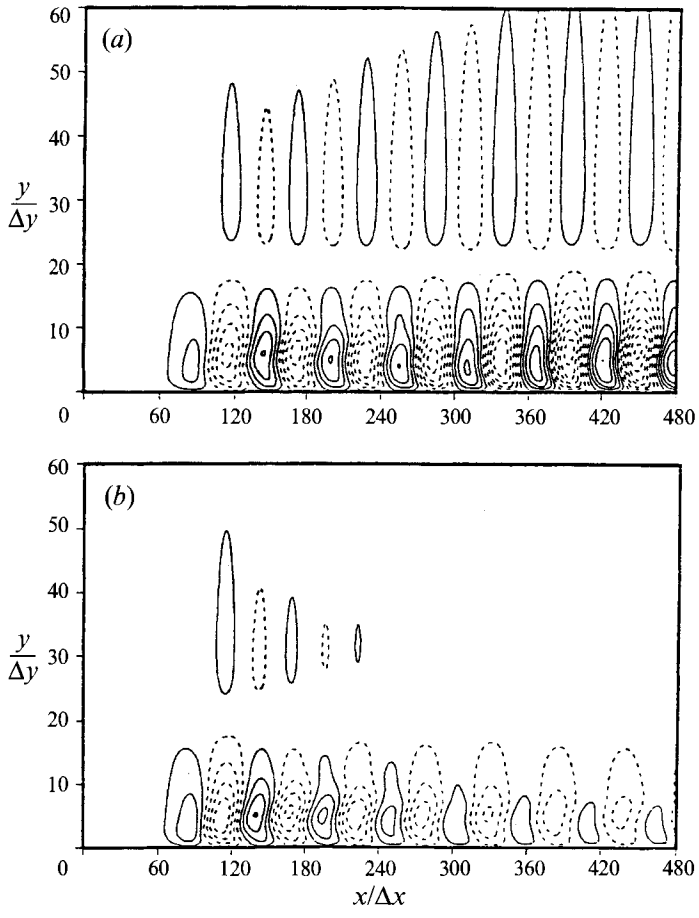

FIGURE 17(*a*, *b*). For caption see facing page.

and for the disturbed flow for $k \leqslant 1$:

$$V_{x_n, y=0, z_k} = \epsilon_{V_k} \bar{V}_w(\xi_n) \sin(\beta_k t), \tag{5.2b}$$

where $\bar{V}_w(\xi_n)$ is represented by a fifth-order polynomial. The strip is located one disturbance wavelength downstream of the left boundary ($x_{SB} = 60$ and $x_{SE} = 120$) and its width is approximately one disturbance wavelength. The disturbance amplitudes ϵ_{V_k} are chosen so that the velocity perturbations create disturbance waves of the same amplitude as observed in the experiments.

The wall has a uniform temperature distribution ($p = 0$) applied to it, as shown by (5.1*a*). The following two cases are considered for the control of the fundamental breakdown process using uniform wall heating ($p = 0$ in (5.1*a*)): $\Delta\bar{T} = 8$ °F and $\Delta\bar{T} = 15$ °F. These two cases are compared with results from an uncontrolled case.

Contours of the streamwise and spanwise disturbance velocities at the spanwise peak locations are shown in figure 17 for both the uncontrolled case (figures 17*a* and 17*c*) and the controlled case with $\Delta\bar{T} = 15$ °F (Figures 17*b* and 17*d*). Negative contour values are indicated by the dashed lines, while the positive contours are solid. For the uncontrolled flow, the growth in the streamwise x-direction is evident for both velocity components. In contrast, the uncontrolled case exhibits a strong reduction of disturbance levels when proceeding in the downstream direction.

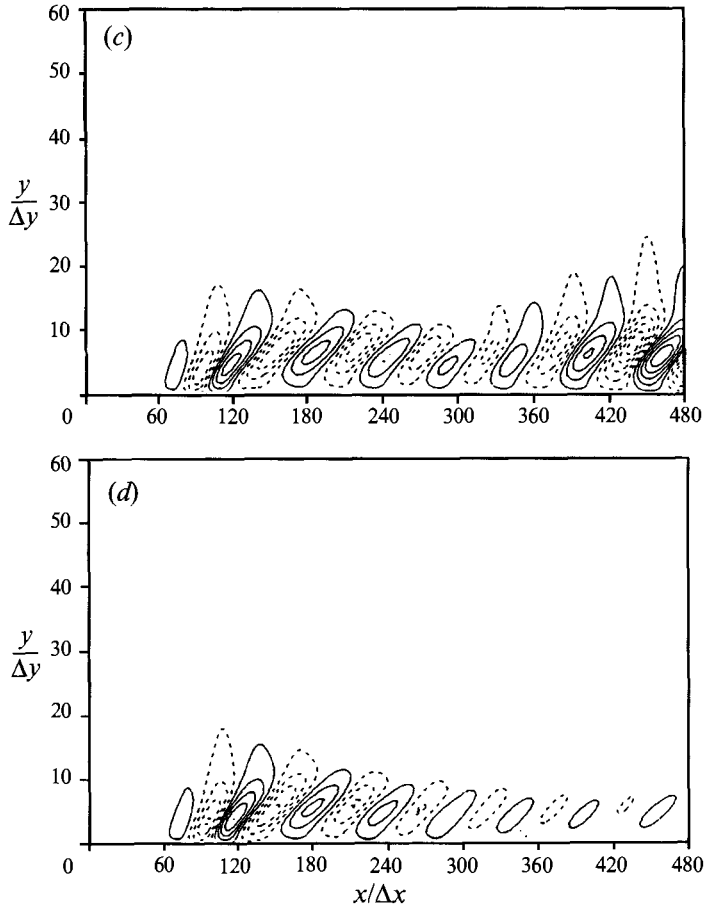

FIGURE 17. Comparison of the disturbed flow for fundamental breakdown without control and with uniform wall heating at the spanwise peak plane. Contours of instantaneous velocity components in the (x, y)-plane are shown for the (*a*) streamwise velocity, u, $z = 0$ and $\Delta\bar{T} = 0$ °F, (*b*) streamwise velocity, u, $z = 0$ and $\Delta\bar{T} = 15$ °F, (*c*) spanwise velocity, w, $z = \frac{1}{4}\lambda_z$ and $\Delta\bar{T} = 0$ °F, and (*d*) spanwise velocity, w, $z = \frac{1}{4}\lambda_z$ and $\Delta\bar{T} = 15$ °F. Contour increments are 0.0023 for the streamwise velocity and 0.0004 for the spanwise velocity.

To examine the influence of uniform heating on the fundamental breakdown process in more detail, amplitude distributions with respect to y are shown in figure 18. The comparison is made for $x = 10.65$. The amplitude distributions are shown for both the fundamental frequency $F_1 = 0.588$ and for the first harmonic $F_2 = 2F_1$ for both the two- and three-dimensional wave components. The reduction in amplitude is clearly evident for both the fundamental and higher harmonic. The U_0 velocity component with fundamental frequency F_1 shows similar trends as observed in the linear control results. The shape of the amplitude profiles are not strongly affected. As seen from the results for the case $\Delta\bar{T} = 15$ °F, increased heating appears not to have as strong an effect as might be expected for this high temperature when compared with the $\Delta\bar{T} = 8$ °F case. This is probably due to the fact that the viscosity does not vary as strongly with temperature at the higher temperature levels. For the first harmonic F_2 of the U_0 velocity shown in figure 18(*b*), the amplitude level shows an even stronger reduction. In addition, the amplitude profiles show a certain change in shape and a third

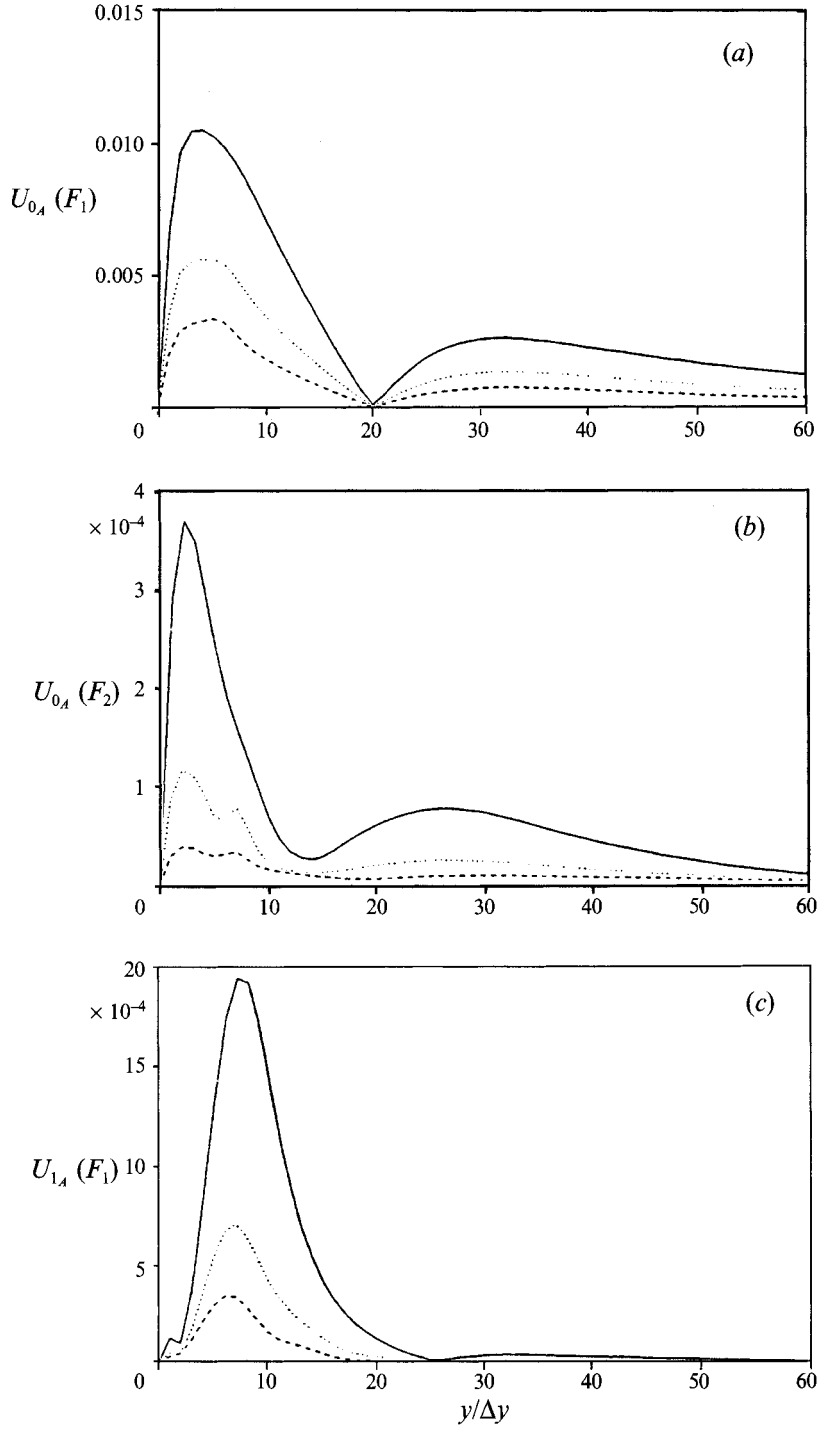

FIGURE 18(*a–c*). For caption see facing page.

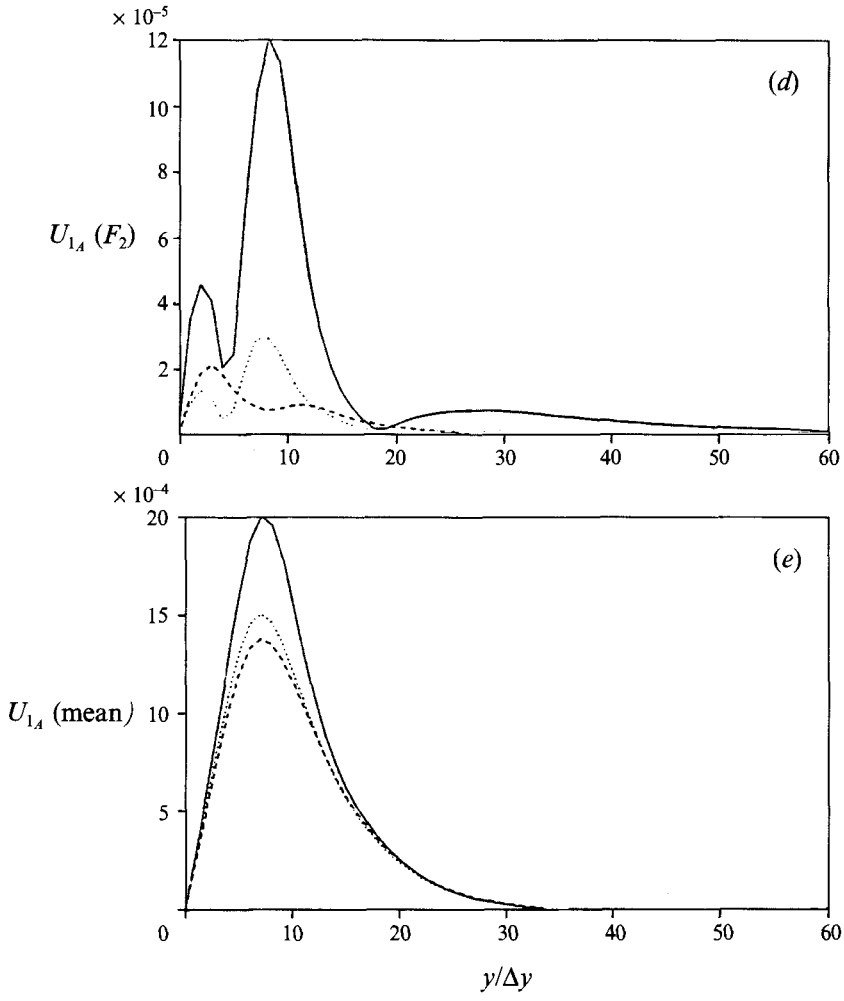

FIGURE 18. Influence of uniform wall heating on the amplitude distribution at $x = 10.65$ and $z = 0$ (spanwise peak plane) for fundamental breakdown on the (*a*) two-dimensional streamwise velocity, U_0, $F_1 = 0.588$, (*b*) two-dimensional streamwise velocity, U_0, F_2, (*c*) three-dimensional streamwise velocity, U_1, F_1, (*d*) three-dimensional streamwise velocity, U_1, F_2, and (*e*) three-dimensional streamwise velocity, U_1, mean component. ——, $\Delta\bar{T} = 0$ °F; ..., 8 °F; – – –, 15 °F.

maximum appears for the lower amplitudes. Figure 18(*c*) shows the effect of uniform heating on the U_1 velocity (three-dimensional component) for the fundamental frequency F_1. Here the influence of uniform heating is more significant. The amplitudes are more strongly reduced than for the two-dimensional component. The amplitude profiles for the first harmonic of the U_1 velocity are shown in figure 18(*d*) and the reduction in amplitude is again evident. The location of the main peak is also shifted closer to the wall when heating is applied. Finally, figure 18(*e*) shows the three-dimensional mean component. This is the time invariant, three-dimensional component which is periodic in the spanwise direction. This component represents a stationary modulation of the base flow and was first observed in the experiments of Klebanoff *et al.* (1962). This stationary component is present for all flow variables and represents a longitudinal vortex system. This three-dimensional mean component creates the peak–valley structure. This component is on the same order of magnitude as the three-

dimensional component with the fundamental frequency for the uncontrolled case. It is obvious from figure 18(*e*) that the time invariant component is not significantly reduced with heating applied when compared with the reduction in amplitudes of the fundamental and first harmonic; in particular additional heating from 8° to 15° has only an insignificant effect.

To further explore the behaviour of the spanwise periodic mean flow component, the U_1 mean component is plotted versus the streamwise x-direction in figure 19(*a*). The amplitudes are for the maximum of the U_1 mean velocity. For the uncontrolled flow, this mean component develops rapidly downstream and shows a significant increase in growth rate towards the end of the x-domain under consideration. However, for the heated boundary layer, this mean component begins to decrease near the end of the domain of interest. Thus heating is also reducing the strength of the longitudinal vortex system. For the fundamental frequency, figures 19(*b*) and 19(*c*) show the streamwise amplitude growth for the U_0 and U_1 velocities, respectively. The two-dimensional amplitude shows a growth downstream for the uncontrolled case, but is clearly damped with heating applied. The three-dimensional amplitude without passive control applied shows a reduction in growth downstream and then a very sharp increase in the growth rate as secondary instability strongly sets in. A solution of the Orr–Sommerfeld equation for three-dimensional disturbances shows that a linear-amplitude wave should decay over the Reynolds number region considered here. The strong three-dimensional growth rate at the end of the domain is therefore probably due to nonlinear effects. With heating applied, the three-dimensional amplitude levels and growth rates are reduced. Although the three-dimensional growth rates are positive towards the end of the solution domain, they are much smaller than without control applied.

5.3.2. *Passive control of the subharmonic breakdown process*

Passive control of the subharmonic breakdown process is now discussed and comparison is made with control of the fundamental breakdown process. The parameters used in the numerical simulations are as follows: $F_{2D} = 1.24$ ($\beta_{2D} = 12.4$), $F_{3D} = 0.62$ ($\beta_{3D} = 5.2$), $\gamma = 32.47$, $K = 2$, $\epsilon_{V_0} = 1.45 \times 10^{-3}$, and $\epsilon_{V_1} = 6.00 \times 10^{-6}$. The parameters are chosen to simulate as closely as possible the laboratory experiments of Kachanov & Levchenko (1984). The two-dimensional fundamental frequency is twice the three-dimensional fundamental frequency. There are approximately 30 points per two-dimensional streamwise wavelength and 60 grid points per three-dimensional streamwise disturbance wavelength. The streamwise domain contains approximately 30 two-dimensional disturbance wavelengths and 15 three-dimensional disturbance wavelengths. The normal direction spans ten boundary-layer displacement thicknesses at the inflow boundary and approximately 4.5 boundary-layer displacement thicknesses at the outflow boundary. The time discretization is chosen so that there are 60 timesteps per two-dimensional disturbance period and thus 120 timesteps per three-dimensional disturbance period. Five disturbance periods of the subharmonic wave component (until $L = 600$) are computed. As for the fundamental breakdown case, tests have shown that the parameter $K = 2$ is sufficient to resolve the spanwise flow in the computational region considered.

As in the previous section, the disturbances are introduced through a suction and blowing strip at the wall. The same wall boundary conditions are used to create the disturbance waves as for fundamental breakdown and are given by (5.2). The suction and blowing strip is located between $x_{SB_1} = 50$ and $x_{SE_1} = 110$ and its width is about one (three-dimensional) wavelength. The disturbance amplitudes ϵ_{V_0} and ϵ_{V_1} are chosen

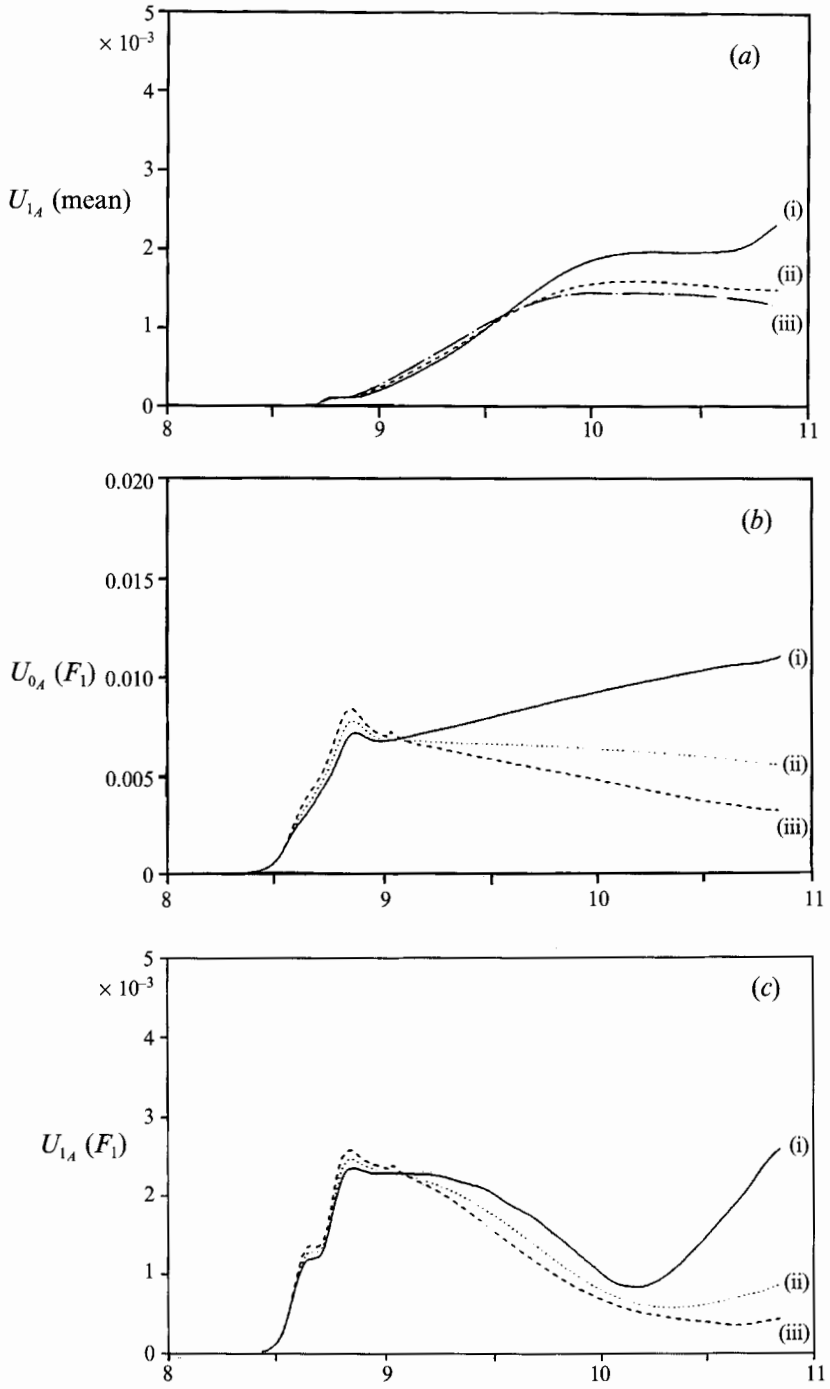

FIGURE 19. Influence of uniform wall heating on the amplitude growth for fundamental breakdown based on the amplitude at (*a*) the maximum of the three-dimensional streamwise velocity, U_1, mean component, (*b*) the maximum of the two-dimensional streamwise velocity, U_0, F_1, and (*c*) the maximum of the three-dimensional streamwise velocity, U_1, F_1. (i) $\Delta\bar{T} = 0$ °F; (ii) $\Delta\bar{T} = 8$ °F; (iii) $\Delta\bar{T} = 15$ °F.

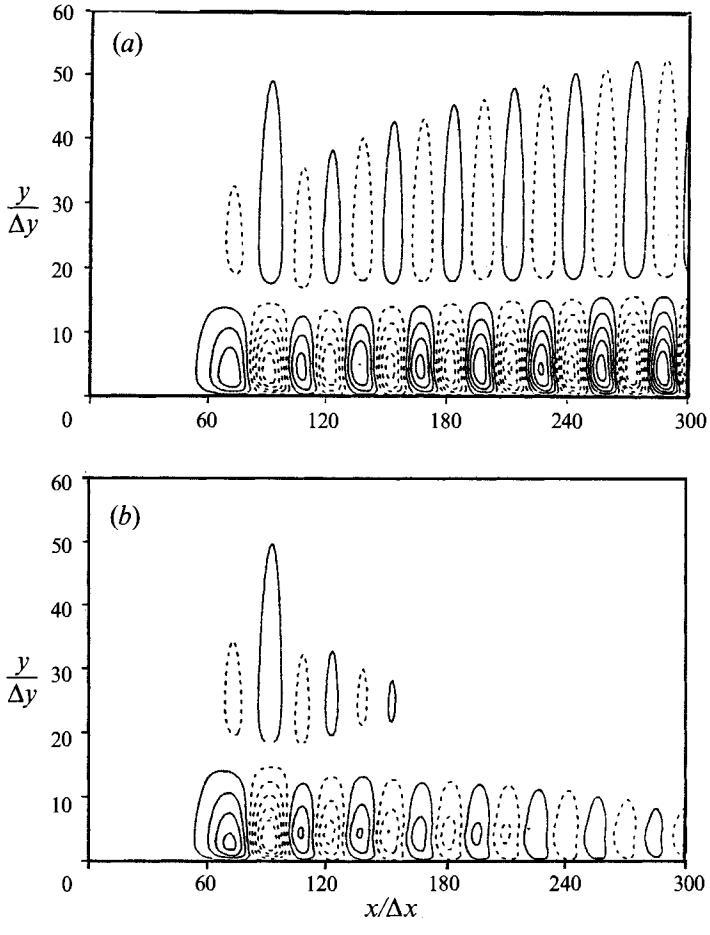

FIGURE 20(*a*, *b*). For caption see facing page.

to match the velocity perturbations observed in the experiments. For the control of subharmonic breakdown, the following two cases are considered: $\Delta\bar{T} = 8$ °F and $\Delta\bar{T} = 15$ °F.

The disturbed flow in the (x, y)-plane at a peak position in the spanwise direction is shown at timestep $L = 600$ in figure 20. Contours are shown for the streamwise and spanwise velocities. Comparison is shown between the uncontrolled flow field $\Delta\bar{T} = 0$ °F and the uniformly heated flow $\Delta\bar{T} = 15$ °F. Comparing the results for the controlled and the uncontrolled cases, it is obvious that there is a significant reduction of amplitude in the downstream direction for the heated flow. In fact, the three-dimensional components are even more reduced than the two-dimensional components. The stationary modulation of the base flow that was present in the fundamental breakdown simulation is not present here. This is consistent with the fact that the subharmonic breakdown does not exhibit a longitudinal vortex system.

The influence of uniform heating on the amplitude profiles for the subharmonic breakdown process is shown in figure 21. Comparison is made at $x = 3.0$. The amplitude profiles for the fundamental frequency and the first harmonic are shown for both the two- and three-dimensional wave components. The U_0 velocity with fundamental frequency $F_1 = F_{2D} = 1.24$ is shown in figure 21(*a*) and shows similar trends as seen in the control of fundamental breakdown. However, heating reduces the

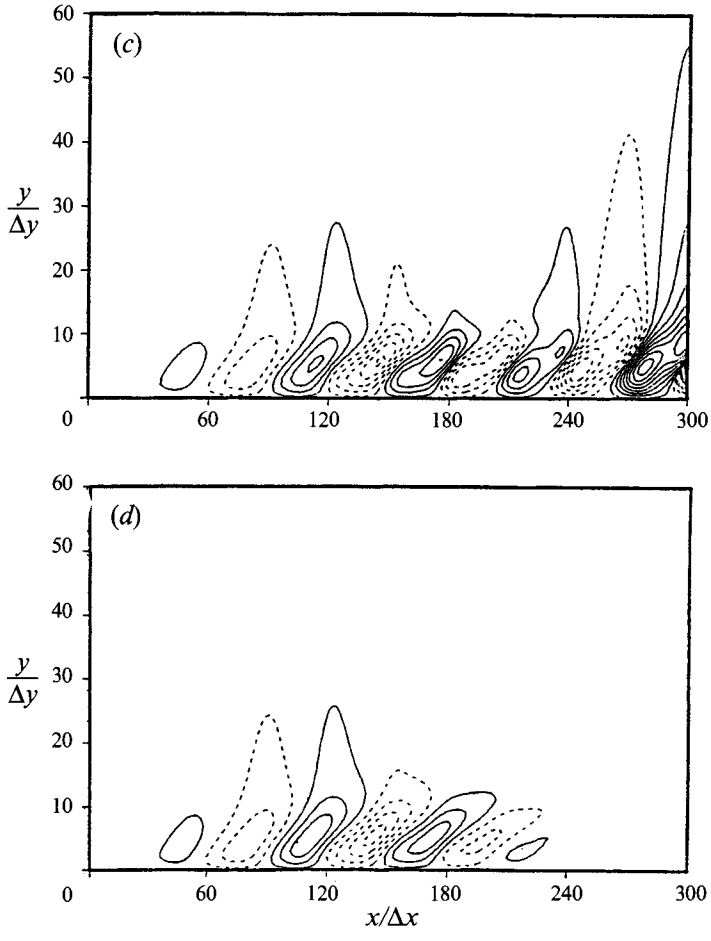

FIGURE 20. Comparison of the disturbed flow for subharmonic breakdown without control and with uniform wall heating at the spanwise peak plane. Contours of instantaneous velocity components in the (x, y)-plane are shown for the (*a*) streamwise velocity, u, $z = 0$ and $\Delta\bar{T} = 0$ °F, (*b*) streamwise velocity, u, $z = 0$ and $\Delta\bar{T} = 15$ °F, (*c*) spanwise velocity, w, $z = \frac{1}{4}\lambda_z$ and $\Delta\bar{T} = 0$ °F, and (*d*) spanwise velocity, w, $z = \frac{1}{4}\lambda_z$ and $\Delta\bar{T} = 15$ °F. Contour increments are 0.002 for the streamwise velocity and 0.000014 for the spanwise velocity.

amplitude levels by a slightly higher level. The subharmonic breakdown is at a different frequency and in a different Reynolds number range than the fundamental breakdown simulations so the stability characteristics of the flow are different. The first harmonic $F_2 = 2F_1$ of the U_0 velocity is shown in figure 21 (*b*). As for the fundamental breakdown cases, the amplitude level of the first harmonic shows an even stronger reduction than the fundamental frequency. The change in shape with heating can again be observed. The influence of uniform heating on the U_1 velocity profile for the three-dimensional fundamental frequency $F_{\frac{1}{2}} = F_{3D} = \frac{1}{2}F_1$ is shown in figure 21 (*c*). As seen in the control of fundamental breakdown, the three-dimensional amplitudes are reduced by a considerably larger percentage than the two-dimensional components. A shift of the maximum towards the wall and the appearance of a second maximum can be observed. Finally, the first harmonic of the U_1 velocity is shown in figure 21 (*d*) for the frequency $F_{\frac{3}{2}} = 3F_{3D} = \frac{3}{2}F_1$. As can be seen, the first harmonic of the three-dimensional U_1 velocity is almost completely damped out for the higher heating level.

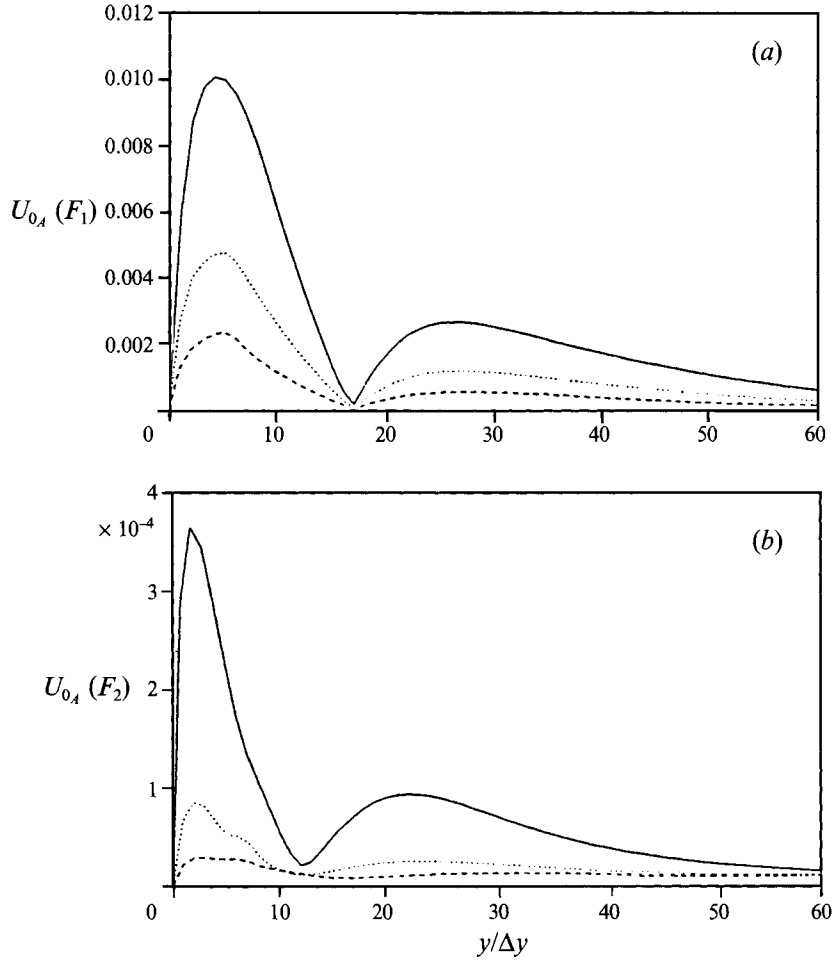

FIGURE 21 (*a*, *b*). For caption see facing page.

The downstream amplitude growth for the subharmonic breakdown case is shown in figure 22 for the maximum of both the U_0 and U_1 velocity components for the two-dimensional fundamental frequency F_1 and the three-dimensional subharmonic frequency $F_{\frac{1}{2}}$. The two-dimensional growth is again similar to that observed in the fundamental breakdown simulations. With uniform heating applied, the disturbances are damped downstream. The behaviour of the three-dimensional disturbance growth is also similar to the fundamental breakdown process. Without control applied, the amplitudes decay slightly and then a strong increase in growth rate appears. As for the fundamental breakdown case, linear stability theory results have shown that small-amplitude three-dimensional disturbances are stable for the Reynolds number range considered here. Therefore, the increased three-dimensional growth is attributed to the secondary instability mechanism. With heating employed, the three-dimensional amplitude levels and growth rates are significantly reduced. The fact that passive control of subharmonic breakdown appears slightly more effective when compared with fundamental breakdown is most probably due to the lower amplitude levels required in the early stages of subharmonic breakdown, as compared to fundamental breakdown.

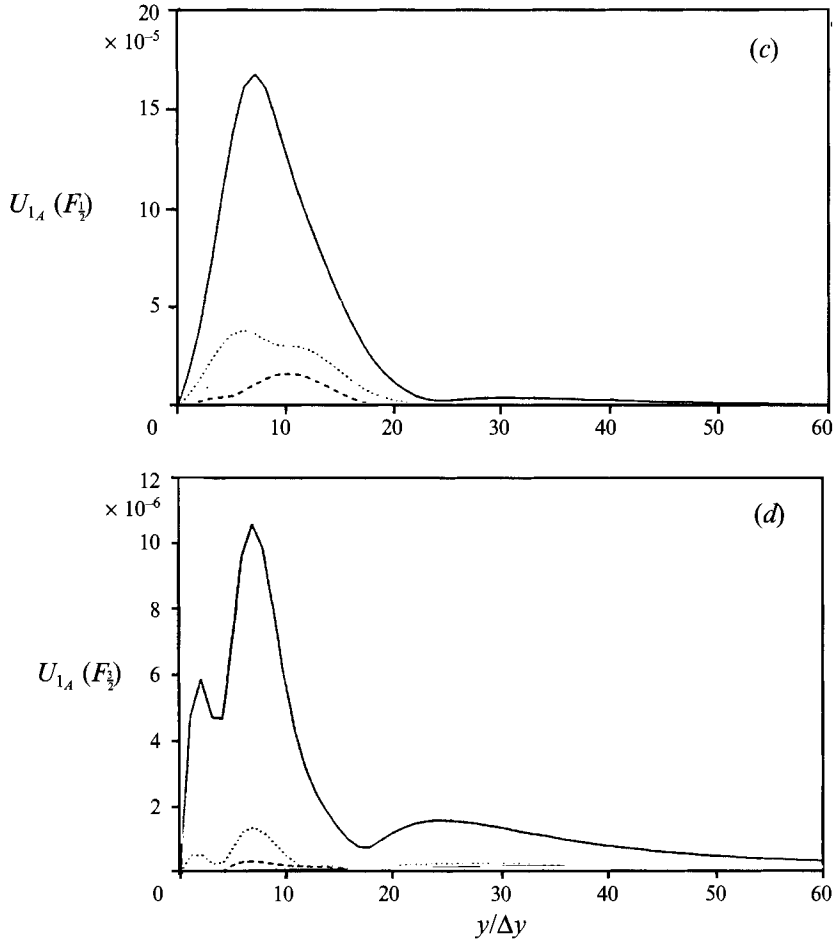

FIGURE 21. Influence of uniform wall heating on the amplitude distribution at $x = 3.0$ and $z = 0$ (spanwise peak plane) for subharmonic breakdown on the (*a*) two-dimensional streamwise velocity, $U_0, F_1 = 1.24$, (*b*) two-dimensional streamwise velocity, U_0, F_2, (*c*) three-dimensional streamwise velocity, $U_1, F_{\frac{1}{2}}$, and (*d*) three-dimensional streamwise velocity, $U_1, F_{\frac{3}{2}}$. See figure 18 for key.

6. Conclusions

A numerical method has been developed for studying passive control of the transition phenomena in a flat plate boundary layer using wall heating. Control of small-amplitude two- and three-dimensional oblique waves was investigated with uniform heating applied. It was shown that the amplitude levels and growth rates can be significantly reduced. Non-uniform surface heating has been shown to be an even more efficient means of controlling linear amplitude disturbance waves, requiring less total heat input than for uniform heating.

Comparison of the small-amplitude control investigations was made with parallel linear theory, non-parallel theory, and experiments. The agreement with the linear theory of Lowell (1974), El-Hady & Nayfeh (1979) and Nayfeh & El-Hady (1980) was generally quite good. The results of the direct simulations were in better agreement with the non-parallel theory of El-Hady & Nayfeh at the lower disturbance frequencies. Agreement with the experiments of Strazisar *et al.* (1977) and Strazisar & Reshotko (1978) was qualitatively good at a moderate frequency. However, the experimental

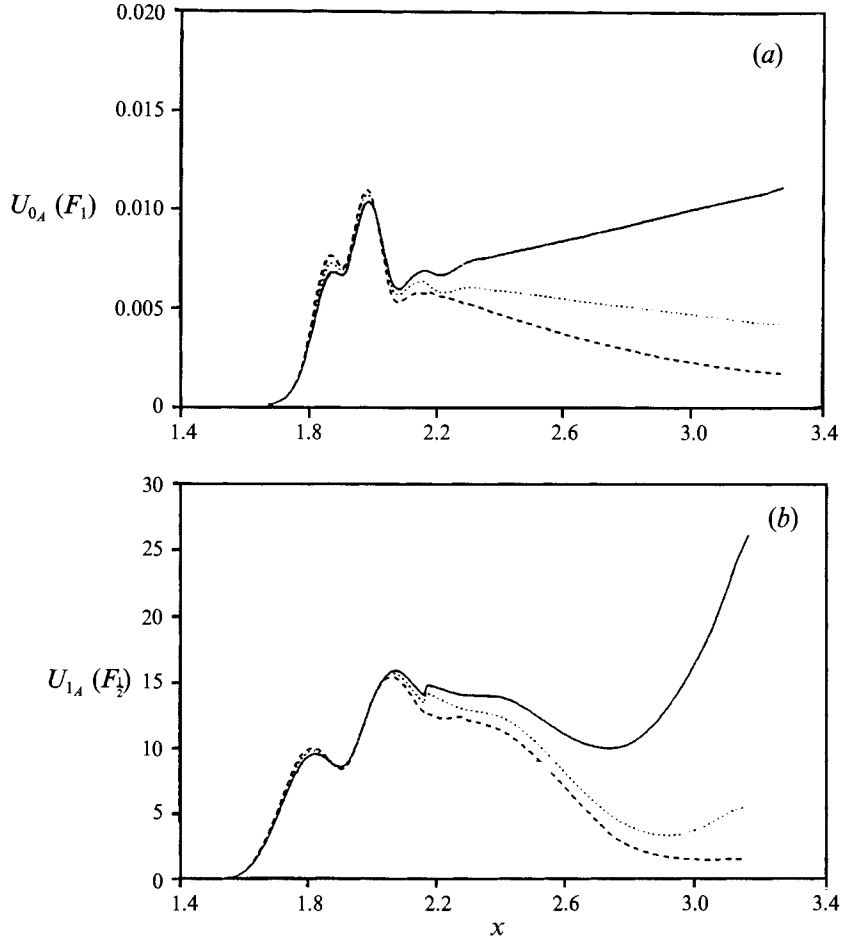

FIGURE 22. Influence of uniform wall heating on the amplitude growth for subharmonic breakdown for (*a*) the maximum of the two-dimensional streamwise velocity, U_0, F_1, and (*b*) the maximum of the three-dimensional streamwise velocity, $U_1, F_{\frac{1}{2}}$. See figure 18 for key.

trends at a higher frequency and larger heating levels, which showed a crossing of the neutral curves, were not predicted by the numerical simulations. However, neither the parallel linear theory nor the non-parallel theory predicted these experimental trends at the higher frequencies.

Control of the secondary instability process was also investigated. Uniform heating for both the fundamental and subharmonic breakdown processes resulted in reductions in the amplitude levels and growth rates for both the two- and three-dimensional components. The level of control achieved was similar for both breakdown processes with control of the subharmonic breakdown process slightly more effective, which is attributed in part to the lower two-dimensional amplitude levels present for subharmonic breakdown. The high three-dimensional growth rates that are characteristic of the secondary instability process were significantly reduced compared to the uncontrolled state.

This research was sponsored by the Office of Naval Research (ONR grant number N00014-N-0515) and the NASA Graduate Student Researchers Program (NASA

grant number NGT-03002809). The computer resources for this work were provided by the NASA Ames Research Center. This support is gratefully acknowledged.

REFERENCES

ASRAR, W. & NAYFEH, A. H. 1985 Nonparallel stability of heated two-dimensional boundary layers. *Phys. Fluids* **28**, 1263–1272.

BARKER, S. J. 1979 Experiments on heat-stabilized boundary layers in a tube. *Proc. 12th Symp. on Naval Hydrodyn.*, pp. 77–85. National Academy of Sciences, Washington, DC.

BARKER, S. J. & JENNINGS, C. 1977 The effect of wall heating upon transition. *Proc. AGARD Symp. on Laminar–Turbulent Transition, Copenhagen*, pp. 19-1–19-9.

BESTEK, H., DITTRICH, P. & FASEL, H. 1987 Einfluß der Wandtemperatur auf die Entwicklung von Tollmien–Schlichting–Wellen in Grenzschichtströmungen. *Z. angew. Math. Mech.* **67**, 256–258.

BUSHNELL, D. M. 1983 Turbulent drag reduction for external flows. *AIAA paper* 83-0227.

BUSHNELL, D. M. & HEFNER, J. N. (eds) 1990 Viscous drag reduction in boundary layers. In *Prog. Astronaut. Aeronaut.* **123** (ed. A. R. Seebass). *AIAA*.

EL-HADY, N. M. & NAYFEH, A. H. 1979 Nonparallel stability of two-dimensional heated boundary layer flows. *Proc. 12th Symp. on Naval Hydrodyn.*, pp. 53–62. National Academy of Sciences, Washington, DC.

FASEL, H. 1976 Investigation of the stability of boundary layers by a finite-difference model of the Navier–Stokes equations. *J. Fluid Mech.* **78**, 355–383.

FASEL, H. 1989 Numerical simulation of instability and transition in boundary layer flows. *Proc. 3rd IUTAM Symp. on Laminar–Turbulent Transition, Toulouse*, pp. 587–598.

FASEL, H. & BESTEK, H. 1980 Investigation of nonlinear, spatial disturbance amplification in plane Poiseuille flow. *Proc. IUTAM Symp. on Laminar–Turbulent Transition, Stuttgart*, pp. 173–185.

FASEL, H., BESTEK, H. & SCHEFENACKER, R. 1977 Numerical simulation studies of transitional phenomena in incompressible, two-dimensional flows. *Proc. AGARD Symp. on Laminar–Turbulent Transition, Copenhagen*, pp. 14-1–14-8.

FASEL, H. & KONZELMANN, U. 1990 Non-parallel stability of a flat plate boundary layer using the complete Navier–Stokes equations. *J. Fluid Mech.* **221**, 311–347.

FASEL, H., RIST, U. & KONZELMANN, U. 1990 Numerical investigation of the three-dimensional development in boundary layer transition. *AIAA J.* **28**, 29–37.

GAZLEY, C. & WAZZAN, A. R. 1985 Control of water boundary layer stability and transition by surface temperature distribution. *Proc. 2nd IUTAM Symp. on Laminar–Turbulent Transition, Novosibirsk*, pp. 153–162.

HAMA, F. R. & NUTANT, J. 1963 Detailed flow observation in the transition process in a thick boundary layer. *Proc. Heat Transfer and Fluid Mech. Inst.* 77. Stanford University Press.

HARDY, R. C. & COTTINGTON, R. C. 1949 *J. Res. NBS* **42**, 573.

HAUPTMANN, E. G. 1968 The influence of temperature dependent viscosity on laminar boundary-layer stability. *Intl J. Heat Mass Transfer* **11**, 1049–1052.

KACHANOV, YU. S. & LEVCHENKO, V. YA. 1984 The resonant interaction of disturbances at laminar–turbulent transition in a boundary layer. *J. Fluid Mech.* **138**, 209–247.

KLEBANOFF, P. S., TIDSTROM, K. D. & SARGENT, L. M. 1962 The three-dimensional nature of boundary-layer instability. *J. Fluid Mech.* **12**, 1–41.

KLOKER, M., KONZELMANN, U. & FASEL, H. 1993 Outflow boundary conditions for spatial Navier–Stokes simulations of transition boundary layers. *AIAA J.* **31**, 620–628.

KONZELMANN, U., RIST, U. & FASEL, H. 1987 Erzeugung Dreidimensionaler, Räumlich Angefachter Störwellen Durch Periodisches Ausblasen und Absaugen in einer Plattengrenzschichtströmung. *Z. angew. Math. Mech.* **67**, 298–300.

KOVASZNAY, L. S. G., KOMODA, H. & VASUDEVA, B. R. 1962 Detailed flow field in transition. *Proc. Heat Transfer Fluid Mech. Institute*, pp. 1–26.

KRAL, L. D. 1988 Numerical investigation of transition control of a flat plate boundary layer. Dissertation, University of Arizona.

KRAL, L. D. & FASEL, H. F. 1991 Numerical investigation of three-dimensional active control of boundary layer transition. *AIAA J.* **29**, 1407–1417.

LIEPMANN, H. W., BROWN, G. L. & NOSENCHUCK, D. M. 1982 Control of laminar–instability waves using a new technique. *J. Fluid Mech.* **118**, 187–200.

LIEPMANN, H. W. & FILA, G. H. 1946 Investigations of effects of surface temperature and single roughness elements on boundary-layer transition. *NACA Rep.* **890**, 587–598.

LOWELL, R. L. 1974 Numerical study of the stability of a heated, water boundary layer. Dissertation, Case Western Reserve University.

NAYFEH, A. H. & EL-HADY, N. M. 1980 Nonparallel stability of two-dimensional nonuniformly heated boundary-layer flows. *Phys. Fluids* **23**, 10–18.

NOSENCHUCK, D. M. 1982 Passive and active control of boundary layer transition. Dissertation, California Institute of Technology.

SARIC, W. S., KOZLOV, V. V. & LEVCHENKO, V. YA. 1984 Forced and unforced subharmonic resonance in boundary-layer transition. *AIAA paper* 84-0007.

SARIC, W. S. & THOMAS, A. S. W. 1983 Experiments on the subharmonic route to turbulence in boundary layers. *Proc. IUTAM Symp. on Turbulence and Chaotic Phenomena in Fluids, Kyoto*, pp. 117–122.

STRAZISAR, A. J. & RESHOTKO, E. 1978 Stability of heated laminar boundary layers in water with nonuniform surface temperature. *Phys. Fluids* **21**, 727–735.

STRAZISAR, A. J., RESHOTKO, E. & PRAHL, J. M. 1977 Experimental study of the stability of heated laminar boundary layers in water. *J. Fluid Mech.* **83**, 225–247.

SWINDELLS, J. F. 1982 NBS, unpublished results. From *CRC Handbook of Chemistry and Physics*, 63rd edn, 1982–83, F-40, CRC Press.

WAZZAN, A. R., OKAMURA, T. T. & SMITH, A. M. O. 1968 The stability of water flow over heated and cooled flat plates. *Trans. ASME* C: *J. Heat Transfer*, February, 109–114.

WAZZAN, A. R., OKAMURA, T. T. & SMITH, A. M. O. 1970*a* The stability of incompressible flat plate laminar boundary layer in water with temperature dependent viscosity. *Proc. Southeastern Seminar on Thermal Sciences*, pp. 184–201.

WAZZAN, A. R., OKAMURA, T. T. & SMITH, A. M. O. 1970*b* The stability and transition of heated and cooled incompressible laminar boundary layers. *Proc. 4th Intl Heat Transfer Conf.*, FC 1.4, pp. 1–11.

ZANG, T. A. & HUSSAINI, M. Y. 1985*a* Numerical experiments on subcritical transition mechanism. *AIAA paper* 85-0296.

ZANG, T. A. & HUSSAINI, M. Y. 1985*b* Numerical experiments on the stability of controlled shear flows. *AIAA paper* 85-1698.